

RESEARCH

Open Access



A constitutive heterochromatic region shapes genome organization and impacts gene expression in *Neurospora crassa*

Andrew T. Reckard¹ , Abhishek Pandeya^{2†} , Jacob M. Voris^{1†} , Carlos G. Gonzalez Cruz¹ , Oluwatosin Oluwadare² and Andrew D. Klocko^{1*}

Abstract

Background Organization of the eukaryotic genome is essential for proper function, including gene expression. In metazoans, chromatin loops and Topologically Associated Domains (TADs) organize genes into transcription factories, while chromosomes occupy nuclear territories in which silent heterochromatin is compartmentalized at the nuclear periphery and active euchromatin localizes to the nucleus center. A similar hierarchical organization occurs in the fungus *Neurospora crassa* where its seven chromosomes form a Rabl conformation typified by heterochromatic centromeres and telomeres independently clustering at the nuclear membrane, while interspersed heterochromatic loci aggregate across Megabases of linear genomic distance to loop chromatin in TAD-like structures. However, the role of individual heterochromatic loci in normal genome organization and function is unknown.

Results We examined the genome organization of a *Neurospora* strain harboring a ~47.4 kilobase deletion within a temporarily silent, facultative heterochromatic region, as well as the genome organization of a strain deleted of a 110.6 kilobase permanently silent constitutive heterochromatic region. While the facultative heterochromatin deletion minimally effects local chromatin structure or telomere clustering, the constitutive heterochromatin deletion alters local chromatin structure, the predicted three-dimensional chromosome conformation, and the expression of some genes, which are qualitatively repositioned into the nucleus center, while increasing Hi-C variability.

Conclusions Our work elucidates how an individual constitutive heterochromatic region impacts genome organization and function. Specifically, one silent region indirectly assists in the hierarchical folding of the entire *Neurospora* genome by aggregating into the “typical” heterochromatin bundle normally observed in wild type nuclei, which may promote normal gene expression by positioning euchromatin in the nucleus center.

Keywords Genome organization, Chromosome conformation, Heterochromatin, *Neurospora crassa*, Gene expression

†Abhishek Pandeya and Jacob M. Voris contributed equally to this work.

*Correspondence:
Andrew D. Klocko
aklocko@uccs.edu

¹Department of Chemistry & Biochemistry, University of Colorado Colorado Springs, Colorado Springs, CO 80918, USA

²Department of Computer Science, University of Colorado Colorado Springs, Colorado Springs, CO 80918, USA



© The Author(s) 2024. **Open Access** This article is licensed under a Creative Commons Attribution-NonCommercial-NoDerivatives 4.0 International License, which permits any non-commercial use, sharing, distribution and reproduction in any medium or format, as long as you give appropriate credit to the original author(s) and the source, provide a link to the Creative Commons licence, and indicate if you modified the licensed material. You do not have permission under this licence to share adapted material derived from this article or parts of it. The images or other third party material in this article are included in the article's Creative Commons licence, unless indicated otherwise in a credit line to the material. If material is not included in the article's Creative Commons licence and your intended use is not permitted by statutory regulation or exceeds the permitted use, you will need to obtain permission directly from the copyright holder. To view a copy of this licence, visit <http://creativecommons.org/licenses/by-nc-nd/4.0/>.

Introduction

Correct genome organization, including proper chromosome folding, is necessary for DNA-templated processes to function normally, including for wild type (WT) control of gene expression [1–5]. Indeed, improper DNA folding altering transcriptional patterns occurs in human cancer cells [6–8]. Eukaryotic genomes hierarchically fold, as DNA molecules wrap around histone octamers to form chromatin fibers, which are extruded into globules (“loops”) by cohesin, and multiple loops compact into Topologically Associated Domains (TADs) [9–17]. TADs of similar transcriptional activity compartmentalize in the nucleus [10, 11, 17]. Specifically, the more open, gene-rich, and actively transcribed euchromatin primarily localizes to the nucleus center, while the silent, gene-poor, and compact heterochromatin is confined to the nuclear periphery [18–20]. Heterochromatin segregation may drive chromatin compartmentalization, although transcriptional activity might force silent genomic loci to the nuclear periphery [19, 21]. In metazoans, the formation of individual chromosome territories – typified by extensive intra-chromosomal contacts – leads to the clustering of heterochromatic regions within chromosomes [22, 23]. In contrast, the independent aggregation of the heterochromatic centromeres and telomeres of fungal chromosomes into a Rabl conformation promotes widespread intra- and inter-chromosomal heterochromatic contacts [9, 24–26]. All told, heterochromatin bundling is a conserved feature of eukaryote genome organization.

Fungi are excellent genome organization models. Fungal genomes are partitioned into euchromatic and heterochromatic regions, resembling the genomes of metazoans, and the heterochromatin of many filamentous fungi, including *Neurospora crassa*, is subdivided into permanently silent constitutive heterochromatin and temporarily silent facultative heterochromatin [27–29]. The adenine and thymine (AT)-rich, gene-poor, and repetitive constitutive heterochromatic regions, comprising ~16% of the *Neurospora* genome, are marked by the tri-methylation of lysine 9 on histone H3 (H3K9me3); this mark is catalyzed by the histone methyltransferase DIM-5 (KMT1) [28, 30–32]. Specific H3K9me3-marked regions found within the seven *Neurospora* chromosomes (“Linkage Groups” [LGs]) include the regional centromeres, the 14 telomeres, and ~200 interspersed heterochromatic regions [28, 32]. In contrast, *Neurospora* facultative heterochromatin is delineated by the subtelomeric di- or tri-methylation of lysine 27 on histone H3 (H3K27me2/3) catalyzed by the SET-7 (KMT6) histone methyltransferase subunit of the Polycomb Repressive Complex 2 (PRC2) [33–35]. In the *Neurospora* three-dimensional (3D) genome organization, as assessed by in-nucleus chromosome conformation capture with high-throughput sequencing (in situ Hi-C),

robust intra- and inter-chromosomal heterochromatic contacts occur across Megabases of linear genomic distance, yet heterochromatin minimally interacts with euchromatin, highlighting the compartmentalization of fungal chromatin [9, 24, 25]. Several Ascomycete fungi cluster heterochromatic regions at the base of TAD-like structures, suggesting heterochromatin aggregation may be a conserved mechanism organizing fungal genomes [9, 24–26, 36]. Further, subtelomeric facultative heterochromatin helps chromosome ends associate with the *Neurospora* nuclear periphery [37]. Together, both heterochromatin types organize the *Neurospora* genome in a Rabl chromosome conformation.

To understand the importance of individual facultative and constitutive heterochromatic regions in *Neurospora* 3D genome organization, we performed chromatin-specific *in situ* Hi-C on a strain deleted of ~47.4 kilobases (kb) within a H3K27me2/3 domain on the LG VI left arm [34], as well as a strain deleted of an ~110 kb H3K9me3 domain on the LG II right arm (“ΔLGIK9het25”). While the H3K27me2/3 deletion minimally impacts genome organization, the ΔLGIK9het25 allele alters the inter-heterochromatic region aggregation, which may increase 3D genome organization variability, and changes the chromatin structure at the deletion site, while nearby AT-rich loci still retain substantial H3K9me3 enrichment. Individual chromosomes in a ΔLGIK9het25 strain are predicted to have qualitatively different 3D structures than those in a WT strain, and numerous genes are upregulated with the LGIK9het25 deletion, possibly due to altered gene positioning within the 3D genome. We conclude that a single constitutive heterochromatic region helps form the “typical” genome organization and promotes normal genome function in WT *Neurospora*.

Materials and methods

Strains and growth conditions

Neurospora crassa strains WT N150 (derived from the strain 74-OR23-IVA [Fungal Genetics Stock Center #2489]), N2930 (mat A his-3; Δmus52::bar⁺), N3944 (mat x; Δdim-5::bar⁺), and N4933 (mat a; Δ47.4 kb::hph⁺) were gifts from Eric U. Selker (University of Oregon). All strains were grown with 1x Vogels minimal medium + 1.5% sucrose and supplements at 32°C [38].

The ΔLGIK9het25 (NKL2) strain, which replaces 110,609 basepairs (bp) of AT-rich DNA in H3K9me3-enriched region number 25 on LG II (between bp 3,602,033 and 3,712,857 of *Neurospora* reference genome version 14 [nc14]) [24] with 1,401 bp of the *P_{trpC}*::hph hygromycin resistance cassette (a net genome deletion of 109,208 bp), was created by split marker gene replacement. Briefly, the ~1,000 bp upstream of LGIK9het25 was PCR amplified with oligonucleotides (“oligos”) oKL14 and oKL15, while the ~1,000 bp downstream

of LGIIK9het25 was amplified with oligos oKL18 and oKL19, by Phusion DNA polymerase (cat# F530-L; ThermoFisher Scientific) using the manufacturer's conditions; oligos oKL15 and oKL18 had ten 5' complementary nucleotides specific to the *P_{trpC}* promoter and *hph* gene 3' end, respectively. Oligo sequences are provided in Table S1. DNA fragments were gel purified using the GenCatch Gel Extraction Kit (cat# 2260250; Epoch Life Sciences), and split marker fragments fusing the LGIIK9het25 upstream to the *P_{trpC}* promoter ("UP"; oKL14 and 2955) or fusing the *hph* gene to the LGIIK9het25 downstream ("DOWN"; oligos 2954 and oKL19) were PCR amplified with the upstream and downstream fragments and a plasmid encoding the *hph* gene (p3xFLAG::hph::LoxP) [39] using LA Taq (cat# RR002M; Takara), and gel purified. The UP and DOWN split marker fragments were transformed into N2930 by electroporation (BioRad MicroPulser Electroporator, cat# 1652100EDU). Hygromycin resistant colonies were selected on 1x Vogels+FGS media with 100 µg/mL hygromycin (cat# ant-hg-5; Invivogen). Genomic DNA was isolated from resultant colonies using standard protocols [40], and tests of proper hygromycin cassette integration at the LGIIK9het25 locus was performed by PCR using oKL49 and 2955 for the left border, 2954 and oKL50 for the right border, and oKL49 and oKL50 for the entire integrated *P_{trpC}::hph* gene. The positive integrant strain tKL1A-2 was crossed to N150 (xKL9AR) and genomic DNA was isolated from hygromycin resistant progeny; similar PCR reactions were performed to confirm the presence of the ΔLGIK9het25 allele in individual cross progeny. PCR with oligos oKL55 and oKL56 determined *Δmus-52::bar* allele absence, and the strain mating type was established by crosses with strains of known mating types. The final homokaryotic strain, NKL2, from cross progeny xKL9AR-17, contains only the ΔLGIK9het25 deletion (NKL2 genotype: *mat A; ΔLGIK9het25::hph*).

Hi-C library construction and bioinformatic analyses

In situ Hi-C was performed as described [24, 25]. Hi-C libraries were Illumina sequenced at the Genomics and Cell Characterization Core Facility (GC3F; University of Oregon), either on a Hi-Seq 2500 as PE100 reads or a NovaSeq 6000 as PE59 reads. For comparison to mutant Hi-C datasets, WT *DpnII* and *MseI* in situ Hi-C datasets (NCBI Gene Expression Omnibus (GEO) accession number GSE173593) [24] were generated by extracting the number of total reads from WT datasets using the sed command for similar numbers of valid reads as mutant datasets. Merged fastq file reads, or individual replicate reads, were mapped with bowtie2 [41] to nc14 [24], or the nc14-derived reference "NKL2 genome" where the LGIIK9het25 sequence is replaced with the *P_{trpC}::hph* sequence. Output sam files were used to build

the initial contact probability matrix at a high [1 kb] resolution with hicExplorer software package [42]. Merged contact probability matrices were used to generate lower resolution contact matrices (hicMergeMatrixBins), compare WT and mutant datasets (hicCompareMatrices), KR correct matrices (hicCorrectMatrix), assess TADs (hicFindTADs [using --correctForMultipleTesting fdr [false discovery rate], --thresholdComparisons 0.3, and --delta 0.15 values for TAD bed files] and hicPlotTADs), and generate images (hicPlotMatrix); replicate similarity was analyzed with (hicCorrelate); additional TAD prediction was performed with Topdom [43]. Chromosome 3D structure prediction was performed with 3DMax (<https://github.com/BDM-Lab/3DMax>) [44] while Neurospora 3D genome structure prediction was performed by LorDG [45], using custom scripts tailored to fungal chromosome biology; scripts are available on the Oluwadare lab GitHub (https://github.com/OluwadareLab/Fungi_3DGenome). Structure prediction contact matrices were made by merging *DpnII* and *MseI* matrices (hicSumMatrices) and converting the .h5 output to NxN text files with a custom script [24] (<https://github.com/Klocko-Lab>). Output PDB files were displayed on ChimeraX [46] with bins containing differentially expressed genes or chromosomal features manually colored, and high-resolution images were used to create figures. PDB files for all 3D structures are available on Zenodo (<https://doi.org/10.5281/zenodo.1124552>).

ChIP-seq library construction and bioinformatic analyses

Chromatin Immunoprecipitation-sequencing (ChIP-seq) was performed as described [47], using anti-H3K9me3 (Active Motif; cat# 39161, lot# 30220003) and anti-H3K27me2/3 (Active Motif; cat# 39535, lot# 23120014) antibodies. All ChIP-seq libraries were Illumina sequenced at the GC3F on a NovaSeq 6000 as SR118 reads. Fastq dataset files were mapped to nc14 or the NKL2 genome with bowtie2 [41], converted to bam files, sorted, and indexed with samtools [48], made into bigwig files with Deeptools [49], and displayed on Integrative Genomics Viewer (IGV) [50], with saved png images used for figure creation. Previously published NCBI GEO or the NCBI Sequence Read Archive (SRA) datasets for WT H3K9me3 (GEO accession numbers GSE68897 and GSE98911), WT H3K27me2/3 (GEO accession numbers GSE68897 and GSE100770), Δ*dim-5* H3K27me2/3 (GEO accession number GSE68897 and SRA accession number SRP058573), and input Neurospora DNA (GEO accession number GSE150758) [32, 51–54], were mapped to the nc14 genome [24] and used to create bigwig files, as above, for image generation on IGV.

Total RNA isolation, polyadenylated RNA-seq library construction, and bioinformatic analyses

Total RNA was isolated from overnight liquid cultures of *Neurospora* strains grown in 1x Vogels, 1.5% sucrose plus supplements [33, 37]. Cultures were harvested by vacuum filtration, placed in 2.0mL screw-top tubes, and 300 μ L of acid washed glass beads suspended in dH₂O (150–212 μ m, Sigma Aldrich cat# G1145-10G), 350 μ L Acid Phenol: chloroform (5:1; ThermoFisher cat# AM9720), and 350 μ L NETS (300mM NaCl, 1mM EDTA, 10mM Tris pH 7.5, 0.2% SDS) were added. Samples were vortexed for 10 min at maximum speed and centrifuged at 4°C for 5 min at 13k rpm. The aqueous layer was transferred to two tubes (~ 250 μ L each), 650 μ L of cold 100% EtOH was added, and RNA was precipitated on ice for 10 min and pelleted by microcentrifugation at 4°C for 10 min at 13k rpm. The pellet was washed with cold 70% EtOH (made with DECP-treated dH₂O), the supernatant was removed, and pellets were allowed to air dry for 15 min and resuspended in 50 μ L DEPC-treated dH₂O. Insoluble material was removed by centrifugation, and the initial RNA concentration was measured by Nanodrop. Total RNA (10 μ g) was resuspended in 50 μ L of DEPC-treated dH₂O, and the Zymo RNA Clean and Concentrator kit (Zymo Research cat# R1013) was used for RNA cleanup per the manufacturer's protocol; the 15 μ L elution was divided into 4 μ L for Qubit concentration (RNA HS assay kit; ThermoFisher Scientific, cat# Q32852) and TapeStation (Agilent) quality control analysis, while the remaining 11 μ L was stored at -80°C. Only total RNA samples with high ribosomal RNA to messenger RNA (mRNA) ratios were used for library construction. Polyadenylated mRNA (polyA mRNA) was selected with the NEBNext Poly(A) mRNA Magnetic Isolation Module (New England Biolabs [NEB], cat# E7490L) and polyA mRNA sequencing libraries were generated with the NEBNext Ultra II Directional RNA Library Prep Kit for Illumina (NEB, cat# E7760L and E7765L) per the manufacturer's protocols; quadruplicate polyA mRNA-seq replicate libraries were constructed for each strain. All polyA mRNA-seq libraries were Illumina sequenced at the GC3F on a NovaSeq 6000 as SR118 reads. Raw fastq files were mapped to the nc14 genome using HiSat2 [55], and htseq-count [56] generated gene count files. Differential Expression analysis between strains was performed with DESeq2 [57] in R/Rstudio [58, 59], selecting significantly changed genes as those with expression $\log_2 > 3.0$ or $\log_2 < -3.0$ and an adjusted p-value < 0.001; bed files for display on IGV were generated from the DESeq2 output gene lists in Microsoft Excel, and volcano plots of \log_2 fold change vs. adjusted p-value were generated in R/R studio.

Results

Loss of a H3K27me2/3-enriched region minimally affects the local chromatin landscape

Since interactions between regions of similar heterochromatin type comprise many of the strongest intra-chromosomal contacts in the *Neurospora* genome [24, 25], we examined how deletions of either type, facultative or constitutive heterochromatin, could impact fungal heterochromatin clustering. Starting with facultative heterochromatin, we examined a previously constructed strain, N4933, originally used to assess position-dependent signals for H3K27me2/3 deposition in the *Neurospora* genome [34]. N4933 harbors a 47.4 kb deletion, from basepairs 175,121 to 222,557 on LG VI, which removes fourteen H3K27me2/3-enriched genes within a larger facultative heterochromatin domain (this strain is named “ Δ K27” for brevity). To assess how Δ K27 impacts genome organization, we performed two *in situ* Hi-C replicates with *Dpn*II to capture chromatin interactions within gene-rich DNA of a higher guanine and cytosine percentage, including in facultative heterochromatic regions. Our replicates show highly similar Hi-C contact matrices across LG VI and are highly correlated (Figure S1), allowing replicate merging into a single Hi-C dataset with 9.2 million (M) valid reads. For comparison, we processed an identical number of valid Hi-C reads from our WT *in situ* *Dpn*II Hi-C dataset [24]. Our initial observation is that, despite having similar valid read numbers, the Δ K27 dataset is slightly biased in capturing more local contacts and less heterochromatin interactions, likely due to variability in Δ K27 Hi-C experiments, with reduced AT-rich heterochromatin ligation, given that the underlying DNA has less *Dpn*II sites. Indeed, decreased inter-centromeric contacts in the Δ K27 dataset, relative to the WT dataset, occur in raw contact matrices (Fig. 1, S2–S3). Inter-centromeric interactions are present upon Knight-Ruiz (KR) [60] correction (Figure S2–S3), indicating capture of biologically relevant structures. However, the decrease in moderate and long-range contacts in the Δ K27 dataset is evident when this contact matrix is directly compared to the WT dataset (Figure S3). Therefore, we focused on the local chromatin changes on LG VI that manifest with the Δ K27 deletion.

On WT LG VI, we observe consistent off-diagonal contacts that decrease with genomic distance, in addition to strong inter-telomeric contacts and the insulation of centromeric DNA from local euchromatin, in both raw and KR corrected heatmaps (Fig. 1A). A higher resolution (5 kb) WT heatmap of the 500 kb surrounding the region targeted for deletion in N4933 shows a similar inverse relationship between contact strength and genomic distance (Fig. 1A). In contrast, the Δ K27 deletion Hi-C, mapped to the *Neurospora* reference genome version 14 (nc14) [24], appears as a white cross emanating from the

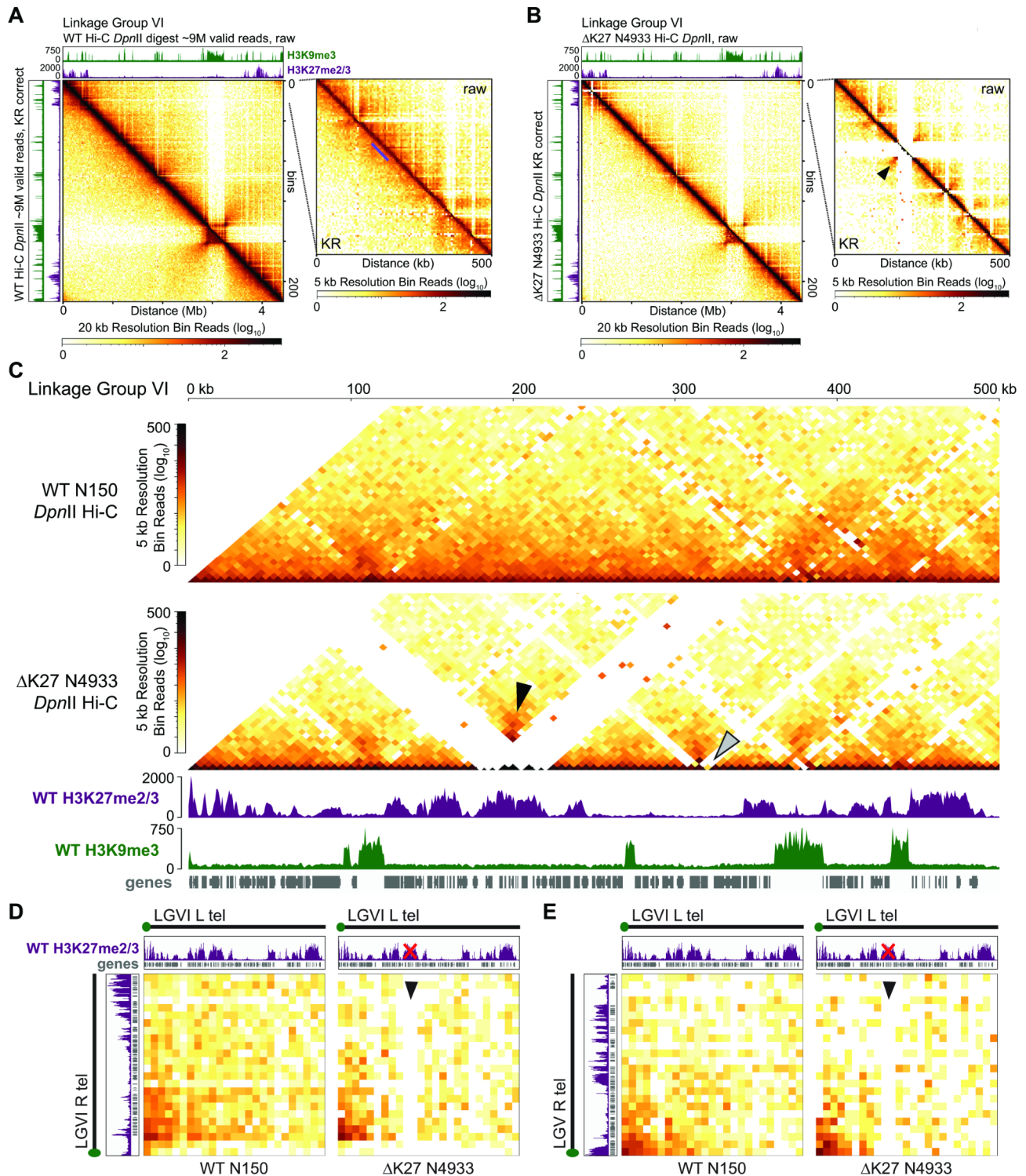


Fig. 1 (See legend on next page.)

deletion locus indicating a gap in mappable Hi-C reads (Fig. 1B), since this DNA was not present during Hi-C ligation capture. This gap occurs in both the raw and KR corrected contact probability heatmaps, although the diagonal base in the KR corrected heatmap presents with

signal (Fig. 1B-C), due to minuscule contact probabilities assigned to bins covering repeated DNA sequences prior to matrix correction (Figure S4); KR correction improperly increases the values of these contact probabilities. Importantly, stronger off diagonal signal at the boundary

(See figure on previous page.)

Fig. 1 A strain harboring a 47.4 kilobase deletion of a H3K27me2/3-enriched domain has minimal genome organization change. **(A-B)** Contact probability heatmaps of *DpnII* (euchromatin-specific) in situ Hi-C datasets at 20 kb resolution across Linkage Group VI (LG VI) of the **(A)** WT or **(B)** N4933 strains, the latter deleted of a 47.4 kb H3K27me2/3-enriched region ("ΔK27"). Enhanced heatmaps show the terminal 500 kb of LG VI, harboring ΔK27, at 5 kb resolution. Each Hi-C image displays the raw contact probability heatmap above the diagonal and the Knight Ruiz (KR) [60] corrected contact probability heatmap below the diagonal; KR correction reduces inherent biases in contact probability matrices. Scalebars shown below the images. Images of wild type H3K9me3 (green) and H3K27me2/3 (purple) ChIP-seq tracks, displayed on IGV [50], above and to the right. The purple line in **(A)** shows the WT location of the H3K27me2/3-enriched region deleted in the ΔK27 strain, while the black arrowhead in **(B)** shows the increased contact probability of flanking euchromatin in ΔK27. **(C)** KR corrected contact probability heatmaps of the *DpnII* in situ Hi-C datasets of WT and ΔK27 strains primarily showing on-diagonal contacts at 5 kb bin resolution. Wild type H3K9me3 ChIP-seq (green), H3K27me2/3 ChIP-seq (purple), and gene (gray) tracks shown below. Scalebar to the left. The black arrowhead shows the increased contact probability of euchromatin flanking the ΔK27 deletion, while the gray arrowhead shows the contact probability loss at a putative transposable element (*sly-1*, gene NCU09969). **(D-E)** Contact probability heatmaps of the WT and ΔK27 telomere interactions, with the **(D)** intra-chromosomal (LG VI left and right telomeres) or **(E)** inter-chromosomal (LG VI left telomere and LG V right telomere) contacts shown. Telomere schematic (with the green circle showing the approximate position of the telomere repeats), and tracks of H3K27me2/3 ChIP-seq (purple) or genes (gray) shown above and right. The red "X" covers the deleted H3K27me2/3 domain, while the black arrowhead shows the deletion site contact depletion

intersections of the facultative heterochromatin deletion appear (Fig. 1B-C, black arrowheads), showing how new interactions occur between the H3K27me2/3-enriched chromatin flanking the ΔK27 deletion. Interestingly, the *sly-1* transposase gene NCU09969 (Fig. 1C, gray arrowhead) is devoid of Hi-C signal in N4933, suggesting the ΔK27 strain had a transposition event. Regarding telomere clustering, the ΔK27 strain still forms intra- and inter-chromosomal subtelomeric contacts (Fig. 1D-E), with strong interactions between the terminal ~ 100 kb of H3K27me2/3-enriched chromatin at chromosome ends. We conclude a deletion of a H3K27me2/3-enriched region minimally impacts the organization of the remaining facultative heterochromatic regions on LGVIL.

Deletion of a ~ 110 kb constitutive heterochromatic region alters silent region clustering

In *Neurospora* nuclei, gene-poor AT-rich constitutive heterochromatin is compartmentalized from gene-rich euchromatin and most facultative heterochromatin [24, 47]. To ask if an individual constitutive heterochromatic region impacts *Neurospora* genome organization and function, we deleted a 110,609 bp H3K9me3-enriched region on LG IIR, aptly called "LGIK9het25" as this region is the 25th constitutive heterochromatic region from the LG II left telomere. We chose to delete this second largest AT-rich region on LG II, since there would be a high probability of observing genome organization changes without compromising chromosome function if the centromere was removed. Using split-marker homologous recombination in a Δ *mus-52* strain [61], we replaced the ~ 110.6 kb LGIK9het25 with a hygromycin resistance gene (hygromycin phosphotransferase; *hph*) controlled by a strong constitutive *trpC* promoter (a *P_{trpC}::hph* cassette; Figure S5A). We note a similar-sized DNA replacement could have more accurately represented the LG II chromosome length, but we wanted to avoid cryptic promoters, repetitive sequences for Repeat-Induced Point Mutation (RIP) [28, 62, 63], or AT-rich DNA sequences forming novel constitutive

heterochromatic regions within the inserted DNA; progressive LGIK9het25 region deletions might have elucidated additional changes to heterochromatic loci bundling patterns. We also attempted other heterochromatic region deletions using the nourseothricin acetyltransferase (*nat1*) resistance gene [64], but did not get primary transformants, possibly due to immediate silencing of the AT-rich *nat1* gene at the targeted constitutive heterochromatic loci. We successfully obtained hygromycin-resistant primary transformants deleted of LGIK9het25 (Δ LGIK9het25), in which 109,208 bp are removed from the *Neurospora* genome, given that *P_{trpC}::hph* inserts 1,401 bp. A hygromycin-resistant progeny from a sexual cross, xKL9AR-17, was characterized by PCR analysis as harboring both the Δ LGIK9het25 allele (Figure S5B) and a wild type *mus-52⁺* allele. The final strain, NKL2 (genotype: *mat A*; Δ LGIK9het25::*hph*), had no noticeable growth defect from a WT strain (Figure S5C-D).

We performed chromatin-specific in situ Hi-C [24], using either *DpnII* to monitor gene-rich chromatin contacts or *MseI* to capture the interactions of AT-rich, gene-poor constitutive heterochromatin. Our Δ LGIK9het25 Hi-C replicates (four *DpnII* and two *MseI* replicates) show highly reproducible and correlated interactions (Figure S6), allowing us to merge replicates into enzyme-specific datasets, with the NKL2 *DpnII* dataset containing 20.6 M valid reads and the NKL2 *MseI* dataset comprising 12.2 M valid reads. All Hi-C datasets display the inter-chromosomal centromeric interactions that occur independently from telomere clusters, indicating capture of biologically relevant structures (Figures S7-S8); these chromosomal features were originally detailed in microscopic observations of fluorescently labeled centromeric and telomeric proteins [25, 37]. As before, we selected similar valid read numbers from previously published WT *DpnII* and *MseI* datasets for comparisons [24].

Compared to a WT *DpnII* Hi-C dataset (Fig. 2A), the deleted LGIK9het25 region appears as a large white "cross" devoid of Hi-C interactions on LGII in the NKL2

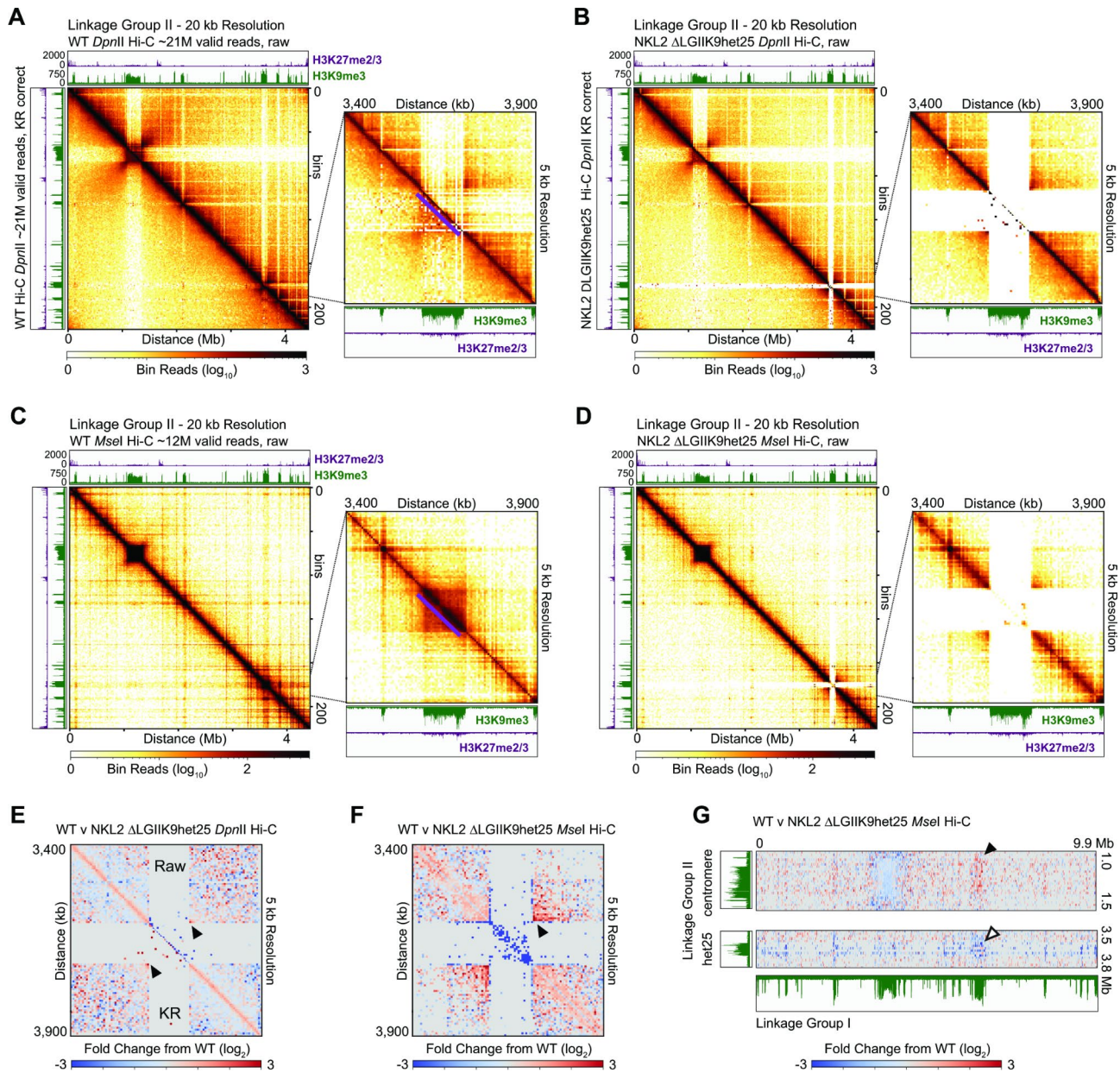


Fig. 2 A ~110 kb H3K9me3-enriched domain deletion alters constitutive heterochromatin region clustering. **(A-D)** Contact probability heatmaps, presented as in Fig. 1, of **(A-B)** *DpnII* (euchromatin-specific) and **(C-D)** *MseI* (heterochromatin specific) *in situ* Hi-C datasets at 20 kb resolution across LG II of **(A, C)** WT or **(B, D)** NKL2 strains, the latter deleted of the 25th H3K9me3-enriched region from the LG II left telomere ("ΔLGIIK9het25"). The purple line in A shows the deleted ΔLGIIK9het25 region. Enhanced (5 kb) resolution heatmaps show the 500 kb surrounding the ΔLGIIK9het25 allele, as in Fig. 1A-B. **(E-F)** Images showing the \log_2 change in Hi-C contact probability between WT and ΔLGIIK9het25 strains in **(E)** *DpnII* (euchromatin-specific) or **(F)** *MseI* (heterochromatin-specific) 5 kb resolution datasets over the 500 kb surrounding the ΔLGIIK9het25 allele. The scalebar of contact probability changes is shown below. **(G)** Images showing the change in inter-chromosomal *MseI* Hi-C contact probability between LG I and the (top) LG II centromere or (bottom) LG II and LG I ΔLGIIK9het25 interspersed heterochromatic region

DpnII contact probability matrix (Fig. 2B). Looking specifically at a 500 kb region surrounding LGIIK9het25, the WT dataset has extensive intra-heterochromatic interactions within LGIIK9het25, and less prominent, but present, heterochromatin-euchromatin contacts (Fig. 2A). In contrast, the NKL2 has contact probability loss, as few interactions occur in the raw interaction heatmap

and sparse contacts at the diagonal in the KR corrected dataset (Fig. 2B), which, like the ΔK27 datasets (Figure S4), is due to a few reads in both the ΔLGIIK9het25 *DpnII* and *MseI* datasets mapping to repetitive DNA sequences present in LGIIK9het25, within the nc14 reference genome, incorrectly increasing contact probability values (Figure S9). The Hi-C contacts surrounding

Δ LGIK9het25 in NKL2 appear enhanced, as the flanking euchromatin moderately gains contacts in the NKL2 *DpnII* dataset, relative to a WT dataset (Fig. 2A-B). Similar contact probability changes occur in WT and NKL2 *MseI* datasets, where in the WT dataset the LGIIK9het25 region extensively contacts internal heterochromatin yet is isolated from surrounding euchromatin, but the NKL2 dataset loses intra-LGIIK9het25 heterochromatic contacts yet gains flanking euchromatin interactions (Fig. 2C-D). Direct comparison of the WT and NKL2 *DpnII* and *MseI* datasets surrounding LGIIK9het25 shows the contact probability gain between flanking euchromatic regions when this separating heterochromatic region is deleted (Fig. 2E-F, arrowheads). The surrounding euchromatin may gain local, on-diagonal interactions, as shown in the *MseI* comparison (Fig. 2F), possibly due to either reduced heterochromatic interactions or a local contact capture bias in the NKL2 dataset. Between LG I and LG II, the LGIIK9het25 deletion causes a loss of inter-heterochromatic region contacts, including from the largest non-centromeric heterochromatic region on LG I (Fig. 2G, white arrowhead), while the LG II centromere loses inter-centromeric contacts but modestly gains interactions with interspersed heterochromatic regions (Fig. 2G, black arrowhead). Similar gains in inter-heterochromatic region interactions are evident across the genome in the NKL2 *MseI* Hi-C dataset, when compared to the WT *MseI* dataset (Figure S10), implying a dramatic shift in the heterochromatin bundle with LGIIK9het25 deletion. When comparing the NKL2 *DpnII* contact matrix to that of a WT strain, the inter-chromosomal contact strength between centromere-proximal euchromatin and more-distant euchromatin on chromosome arms is increased, yet chromosome-internal euchromatic contacts are reduced (Figure S11), consistent with altered bundling between centromeres and interspersed heterochromatic regions. Similarly, both Δ LGIK9het25 Hi-C datasets have depleted inter-centromeric contacts; KR correction reduces *DpnII* contact biases (Figures S10-S11). While it is possible that the LGIIK9het25 deletion causes significant genome organization changes, these results may also highlight moderate levels of variability in the Hi-C data derived from the population of nuclei in the NKL2 strain source tissue. Here, valid genome organization differences would be amplified by subtle disparities in Hi-C experiments. These biases occurred despite our use of the same *in situ* Hi-C protocol to generate highly correlated NKL2 replicates (Figure S6), and how we performed the *DpnII* NKL2 and *MseI* WT Hi-C experiments at the same time, which hypothetically would minimize experimental bias.

To assess changes between the WT and NKL2 strains independent of Hi-C restriction enzymes and to compare datasets generated at the same time, we summed

the *DpnII* and *MseI* datasets from each strain and compared the summed contact probability matrices. The WT and NKL2 summed datasets are similar, with more complete coverage in heterochromatic regions (Fig. S12A-B), yet moderately distant contacts in the NKL2 dataset are reduced. Direct comparison of the summed matrices showed the NKL2 dataset with more local contacts and reduction of more distant interactions, with the loss of contacts within the LGIIK9het25 region readily apparent (Figure S12C). Thus, even when some Hi-C experiments performed at the same time are assessed, variation in contact probability, hypothetically due to differences in genome organization that are enhanced in individual Hi-C experiments, is evident. All told, the LGIIK9het25 deletion may affect the organization of the entire *Neurospora* genome.

The LGIIK9het25 deletion still allows H3K9me3 deposition at nearby AT-rich loci but alters TAD-like structures

Upon deleting LGIIK9het25, the possibility exists that genome function, specifically H3K9me3 deposition on nearby AT-rich loci, is impacted. To assess if LGIIK9het25 loss prevents histone PTM enrichment on surrounding heterochromatic regions, we performed H3K9me3-specific Chromatin Immunoprecipitation-sequencing (ChIP-seq) on the NKL2 strain. The two NKL2 H3K9me3 ChIP-seq replicates are highly reproducible (Figure S13) for merging into a single file that was normalized by Reads Per Kilobase per Million (RPKM) for direct comparison to previously published WT H3K9me3 ChIP-seq datasets, although using spike-in DNA controls in ChIP-seq experiments performed at the same time may be the best practice for assessing strain differences or relative enrichment levels [65, 66]. We mapped the ChIP-seq reads to either the nc14 WT genome or a “NKL2 genome”, a reference genome in which the *P_{trpC}::hph* sequence replaces the AT-rich DNA of LGIIK9het25; enhanced images show low levels of background signal across the *P_{trpC}::hph* sequence in an NKL2 H3K9me3 ChIP-seq dataset that are absent in WT H3K9me3 dataset when both datasets are mapped to the NKL2 reference genome (Figure S5E).

LG II exhibits an identical pattern of absolute H3K9me3 ChIP-seq enrichment across the AT-rich regions surrounding LGIIK9het25, independent of the reference genome used for mapping reads; here, we define “absolute H3K9me3 enrichment” as the presence or absence of this histone PTM at historical AT-rich, gene poor sites originally observed in the WT N150 parent strain. For ChIP-seq data mapped to the WT nc14 genome, identical H3K9me3-enriched regions are observed in both strains, except peaks to the right of LGIIK9het25 are shifted by ~110 kb from the deletion site in the NKL2 strain (Fig. 3A), since positions of these genomic elements in

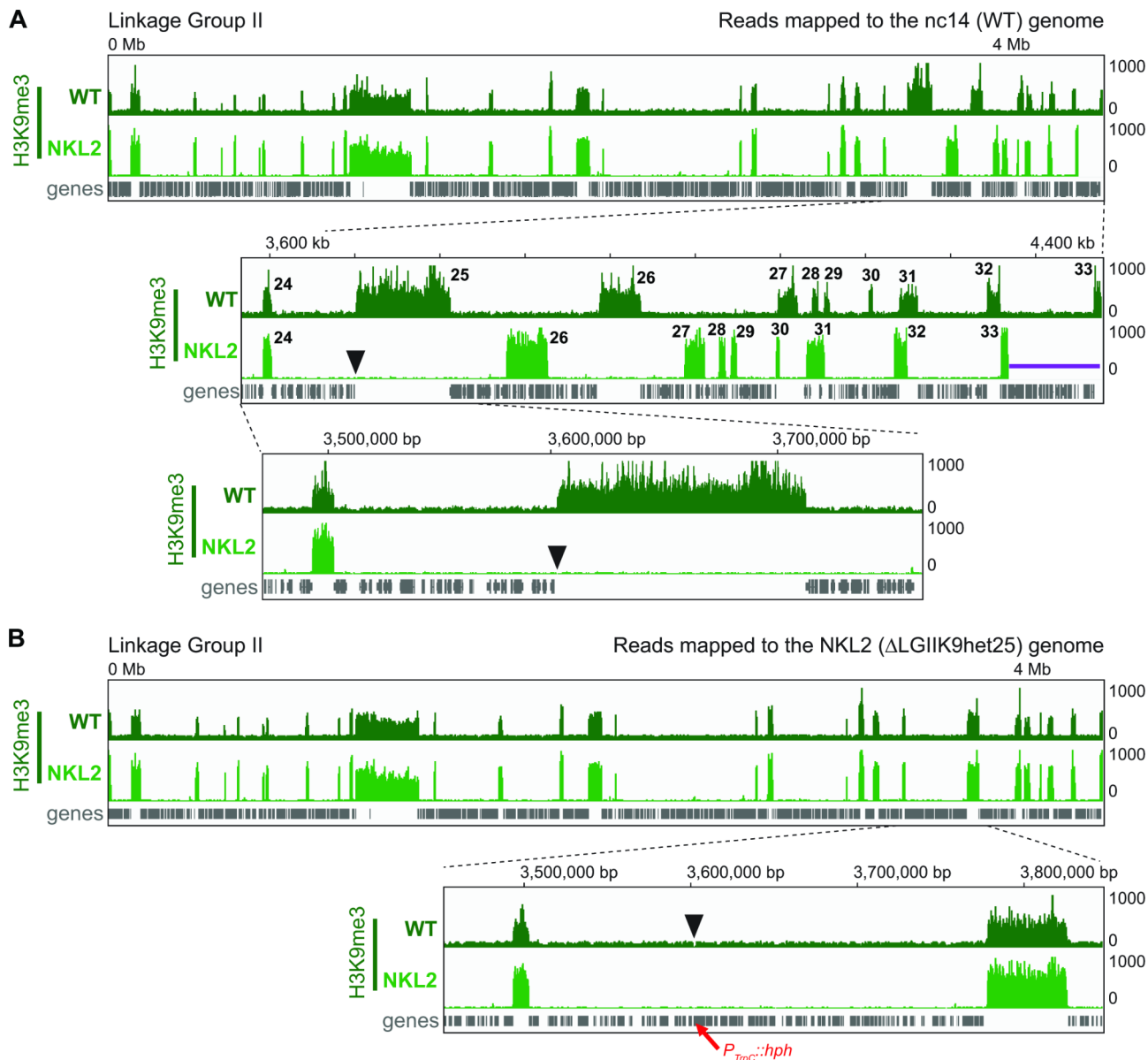


Fig. 3 The LGIIK9het25 deletion does not compromise H3K9me3 deposition at other constitutive heterochromatic regions in the NKL2 strain. **(A–B)** Images of WT (dark green) or NKL2 Δ LGIK9het25 (light green) H3K9me3 ChIP-seq and gene (gray) tracks, displayed on IGV, of the entire LG II chromosome or enhanced regions. H3K9me3 ChIP-seq reads were mapped to the **(A)** WT nc14 or **(B)** NKL2 Δ LGIK9het25 reference genomes. Numbers in the Fig. 3A enhanced panel count the heterochromatic regions from the LG II left telomere, while the black arrowheads show the LGIIK9het25 DNA deletion. The purple line shows the \sim 110 kb of DNA missing from the NKL2 genome (shifting all H3K9me3 peaks to the right of the deletion by \sim 110 kb). The red arrow in B shows the position of the inserted $P_{trpC}::hph$ gene in NKL2

the NKL2 bigwig enrichment count files become shifted when reads in input bam files have altered mapping positions on LG II. Qualitatively, the NKL2 H3K9me3 peaks may be higher (Fig. 3A), possibly reflecting increased H3K9me3 purification from the remaining constitutive heterochromatic regions or enhanced sequencing depth limiting background signal, although we cannot make strict conclusions about relative H3K9me3 enrichment from experiments not performed at the same time. When H3K9me3 ChIP-seq data from both strains is mapped to

the NKL2 reference genome, the H3K9me3 signal loss from LGIIK9het25 in the WT dataset is apparent, while the remaining constitutive heterochromatic regions have identical LG II genomic positions and H3K9me3 enrichment is present (Fig. 3B).

To further assess local chromatin changes resulting from the LGIIK9het25 deletion, we examined TAD-like loop structures on LG IIR. We chose parameters in TAD prediction that mostly placed TAD borders for heterochromatic regions within H3K9me3-enriched domains

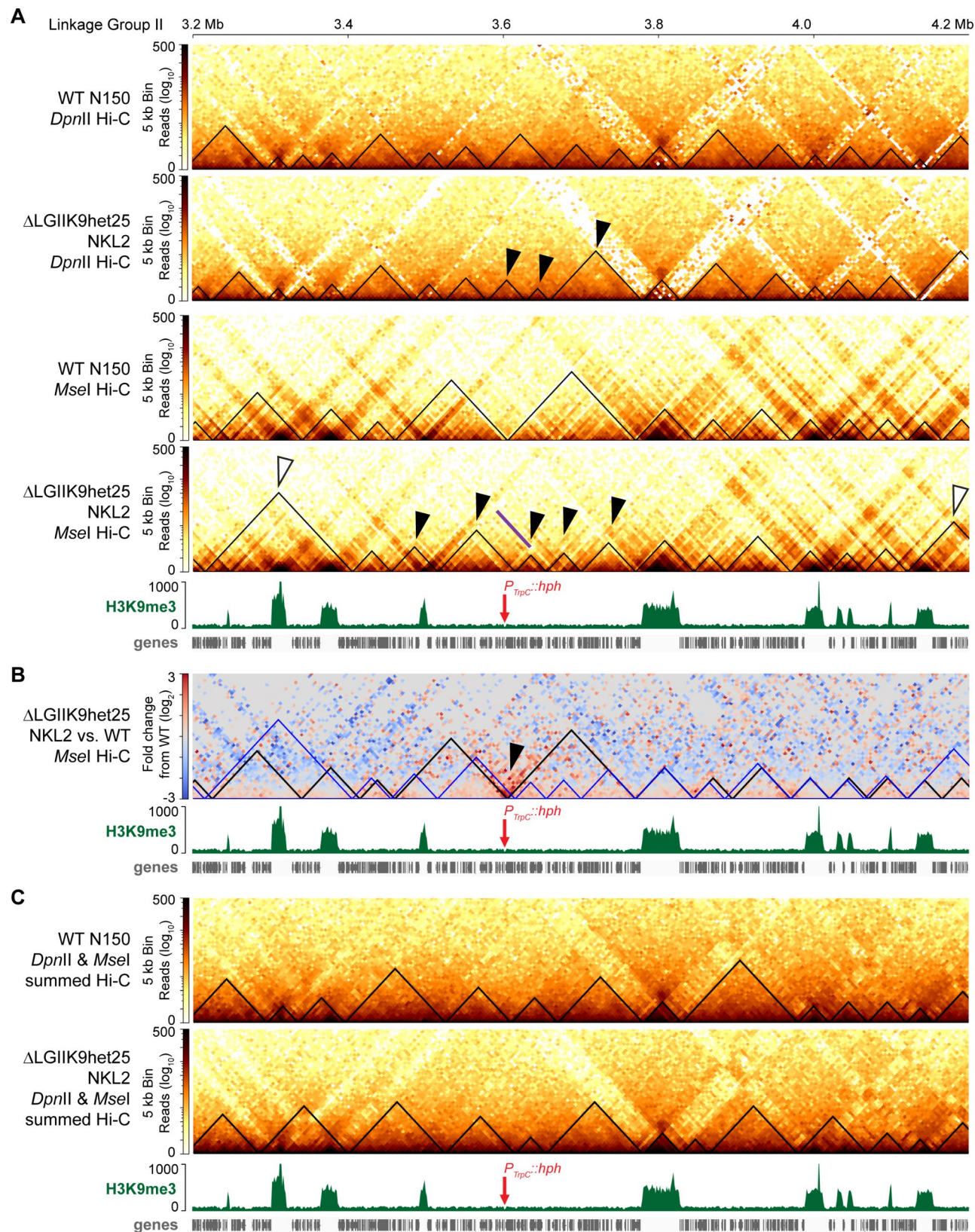


Fig. 4 (See legend on next page.)

(See figure on previous page.)

Fig. 4 The LGIIK9het25 deletion alters the predicted TAD-like structures in the surrounding chromatin. **(A)** Contact probability heatmaps of *DpnII* (KR corrected) or *MseI* (raw) *in situ* Hi-C datasets of WT and Δ LGIIK9het25 strains primarily showing on-diagonal contacts at 5 kb bin resolution, mapped to the NKL2 Δ LGIIK9het25 reference genome. Wild type H3K9me3 ChIP-seq (green) and gene (gray) tracks shown below. The contact probability scale-bar is shown to the left of each heatmap. Predicted TAD-like structures, as determined by hicFindTADs in hicExplorer, are indicated by black triangles. Black arrowheads indicate altered TAD-like structures surrounding the LGIIK9het25 deletion, while white arrowheads show changed TAD-like structures in flanking euchromatin. The red arrow shows the position of the $P_{trpC}::hph$ gene inserted within the NKL2 reference genome, while the purple line shows increased chromatin contacts at the P_{trpC} promoter. **(B)** A heatmap of the changes in contact probability between *MseI* Hi-C datasets of WT and Δ LGIIK9het25 strains, displayed as in A. The TAD-like structures predicted in WT (black) or Δ LGIIK9het25 (blue) strains by hicFindTADs in hicExplorer are shown (triangles). **(C)** Contact probability heatmaps, presented as in A, of WT and Δ LGIIK9het25 strains in which *DpnII* and *MseI* Hi-C dataset were summed prior to KR correction

to increase our chances of predicting biologically relevant TADs, although TAD structure prediction within the same dataset can vary [67]. We started by predicting TAD-like structures in WT and NKL2 *DpnII* and *MseI* datasets mapped to the NKL2 reference genome to examine strain-specific changes in chromatin folding without the LGIIK9het25 deletion signal gap. Clear TAD-like structure changes are observed at the deletion site, with the euchromatin in the NKL2 Δ LGIIK9het25 *DpnII* dataset having larger TAD-like structures, while the NKL2 *MseI* dataset has smaller on-diagonal TAD-like structures (Fig. 4A-B, black arrowheads); this difference likely stems from the chromatin monitored – and the density of restriction sites, with AT-rich heterochromatin having more *MseI* sites – in each Hi-C experiment. The flanking TAD-like structures are nearly identical in both datasets, except for two larger TADs-like structures in the NKL2 *MseI* data (Fig. 4A-B, open arrowheads). The use of Topdom [43] as second TAD prediction program also showed TAD changes in the NKL2 *DpnII* Hi-C data relative to WT (Figure S14A), although the TAD changes differ from those predicted by hicExplorer [42]; the Topdom TADs are highly similar in both WT and NKL2 *MseI* Hi-C datasets (Figure S14B), highlighting the challenges of fungal TAD prediction. Similar TAD-like structure changes across euchromatin are observed in WT and NKL2 *DpnII* datasets mapped to the nc14 (WT) genome, with larger TAD-like structures predicted with the Δ LGIIK9het25 allele, as opposed to the smaller TAD-like structures in WT datasets (Figure S14C). Interestingly, at the $P_{trpC}::hph$ insertion, two novel yet small TAD-like structures are observed in both NKL2 datasets, combined with additional stronger Hi-C interactions in *MseI* data (Fig. 4A, purple line), and comparing the NKL2 contact probability and TADs to those in the WT data highlighted the contact probability increase that alters chromatin folding in NKL2 (Fig. 4B). These data suggest the constitutive P_{trpC} promoter could influence the local contacts and expression of genes in this region. Finally, when TADs are predicted in contact probability heatmaps independent of restriction enzyme used (e.g., in summed *DpnII* and *MseI* contact probability matrices, mapped to either the nc14 or NKL2 reference genomes), subtle TAD changes are seen across the Δ LGK9het25

deletion site despite good agreement between heterochromatin-euchromatin boundaries and TAD borders (Fig. 4C and S14D). Overall, it appears the LGIIK9het25 deletion alters the local chromatin folding surrounding the deletion site.

The LGIIK9het25 deletion alters the three-dimensional folding of *Neurospora* chromosomes

It remains possible that this large constitutive heterochromatic region deletion alters chromosome folding. To assess the 3D folding of LG II, we computationally predicted the LG II 3D structure using WT and NKL2 Δ LGIIK9het25 Hi-C datasets. We chose to merge all *DpnII* and *MseI* data together from each strain to maximize the possible Hi-C contacts across their genomes; we did not combine *DpnII* and *MseI* data at ratios equivalent to the *Neurospora* chromatin distribution, as previously performed [24]. With these summed contact probability matrices, we generated LG II 3D structures using 3DMax [44] customized for biologically relevant structures in fungal genomes; multiple structure prediction iterations occur prior to producing the final 3D structure.

In the WT strain, LG II has an elongated structure with condensed chromosome arms, a more isolated centromere, telomeres localized to a single “side”, and extensive intervening chromatin loops (Fig. 5A). Similar 3D structure prediction changes are observed on the other six WT chromosomes (Figure S15). The LGIIK9het25 region forms a loop and associates with nearby chromatin loops (Fig. 5A), consistent with nine, moderately sized heterochromatic regions present in the terminal 800 kb of the LG II right arm (Fig. 3A). In contrast, the chromosome arms within the LG II 3D structure of the NKL2 LGIIK9het25 deletion are more compact and wider, despite similar centromere isolation, telomere locations, and looping of intervening chromatin (Fig. 5B). However, the terminal right arm of the output 3D structure for NKL2 LG II does not form any loops, which suggests that our requirement for maintaining telomere clusters in fungal 3D structure prediction influences how this NKL2 chromosome folds (Fig. 5B). Similar folding differences occur on each LG in NKL2, with some chromosomes, particularly LG I and LG IV - having drastically altered 3D structures relative to WT (Figures S15, S16).

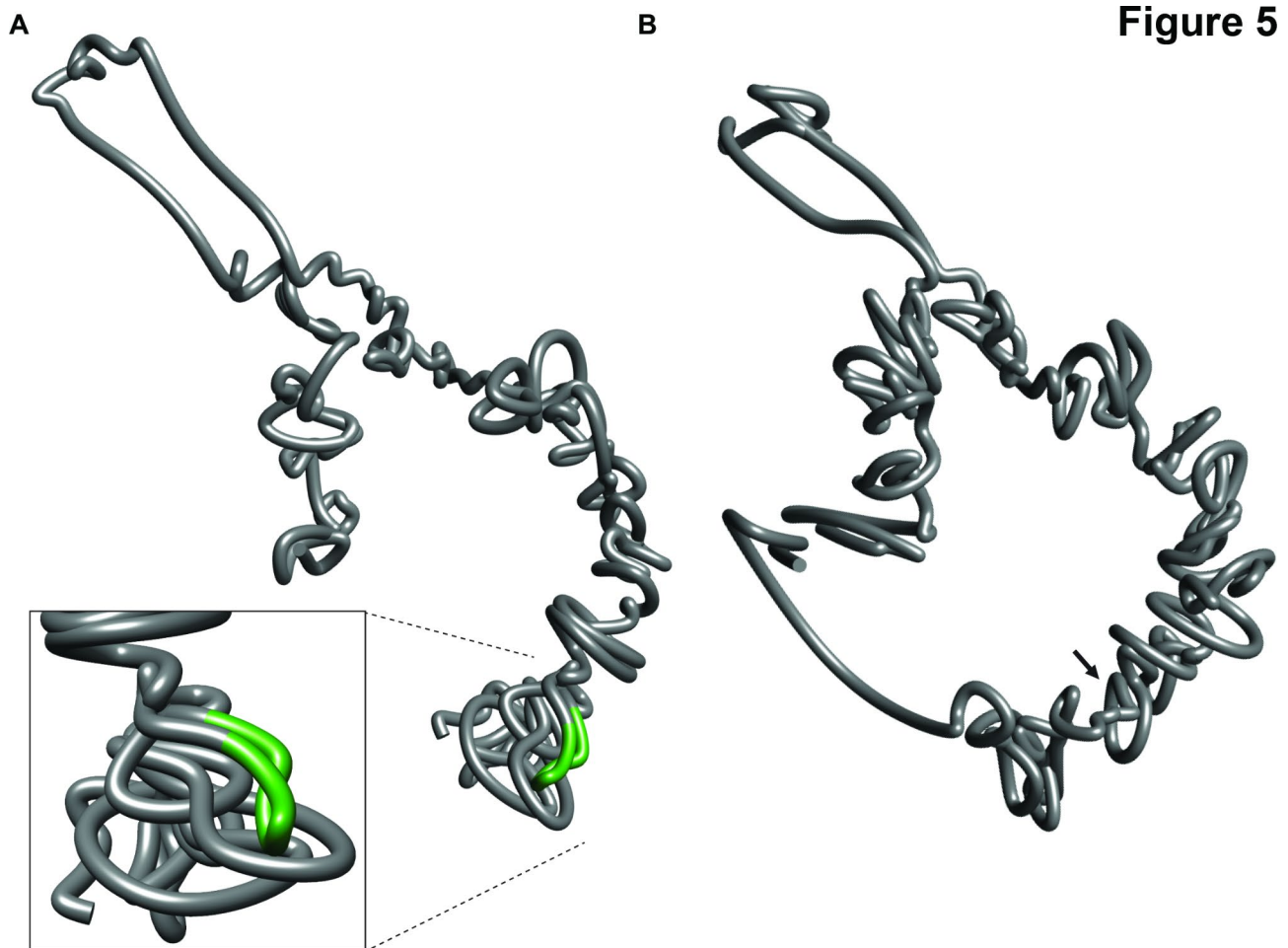


Fig. 5 The predicted 3D folding of a single chromosome is changed with the LGIIK9het25 deletion. **(A-B)** Images depicting the predicted 3D structures of LG II from **(A)** WT or **(B)** NKL2 Δ LGIK9het25 strains at 20 kb resolution. The green region highlights the LGIIK9het25 region in the WT structure. The enhanced image shows the chromatin folding of the LG II right arm surrounding the LGIIK9het25 region in a WT strain. The arrow shows the LGIIK9het25 deletion site

Together, the LGIIK9het25 deletion modifies the predicted 3D structures of *Neurospora* LGs.

The LGIIK9het25 deletion alters gene expression, which is correlated to differences in 3D genome folding

To understand if the removal of LGIIK9het25 could influence genome function by altering gene expression, we assessed changes in polyadenylation messenger RNA sequencing (polyA mRNA-seq) in WT and NKL2 strains. As a control for complete loss of constitutive heterochromatin function, we examined gene expression changes in a Δ dim-5 strain devoid of H3K9me3 genome-wide [30]. Volcano plots displaying the significant gene expression changes ($\log_2 > 3.0$ or < -3.0 ; adjusted p-value < 0.001) in the NKL2 strain relative to the WT strain show 84 genes become significantly upregulated and no genes significantly downregulated, (Fig. 6A, left; Supplementary File S1); additional differentially expressed genes (DEGs) could be identified with less stringent cutoff values. In

contrast, the Δ dim-5 strain has 175 DEGs compared to WT, and many genes have either increased or decreased transcription (Fig. 6A, right; Supplementary File S2), including the strong reduction of the gene NCU04402 encoding DIM-5 (Fig. 6B), confirming the Δ dim-5 strain genotype. Many Δ dim-5 DEGs are found within altered H3K27me2/3 peaks (Figure S17) to possibly explain these transcriptional changes, as facultative heterochromatin relocates to constitutive heterochromatic regions in a Δ dim-5 strain [51, 52]. The Δ LGIK9het25 and Δ dim-5 datasets each have unique DEGs, as only 25 DEGs overlap both datasets. Notably, Δ LGIK9het25 causes less drastic expression changes relative to the Δ dim-5 polyA mRNA-seq (Fig. 6A-B). Further, no DEGs in the Δ LGIK9het25 dataset regulate chromatin or transcription (Supplementary File S3), although many DEGs are hypothetical genes without defined functions, preventing a complete tally of the putative regulatory genes. Interestingly, gene expression changes in the Δ LGIK9het25 strain occur

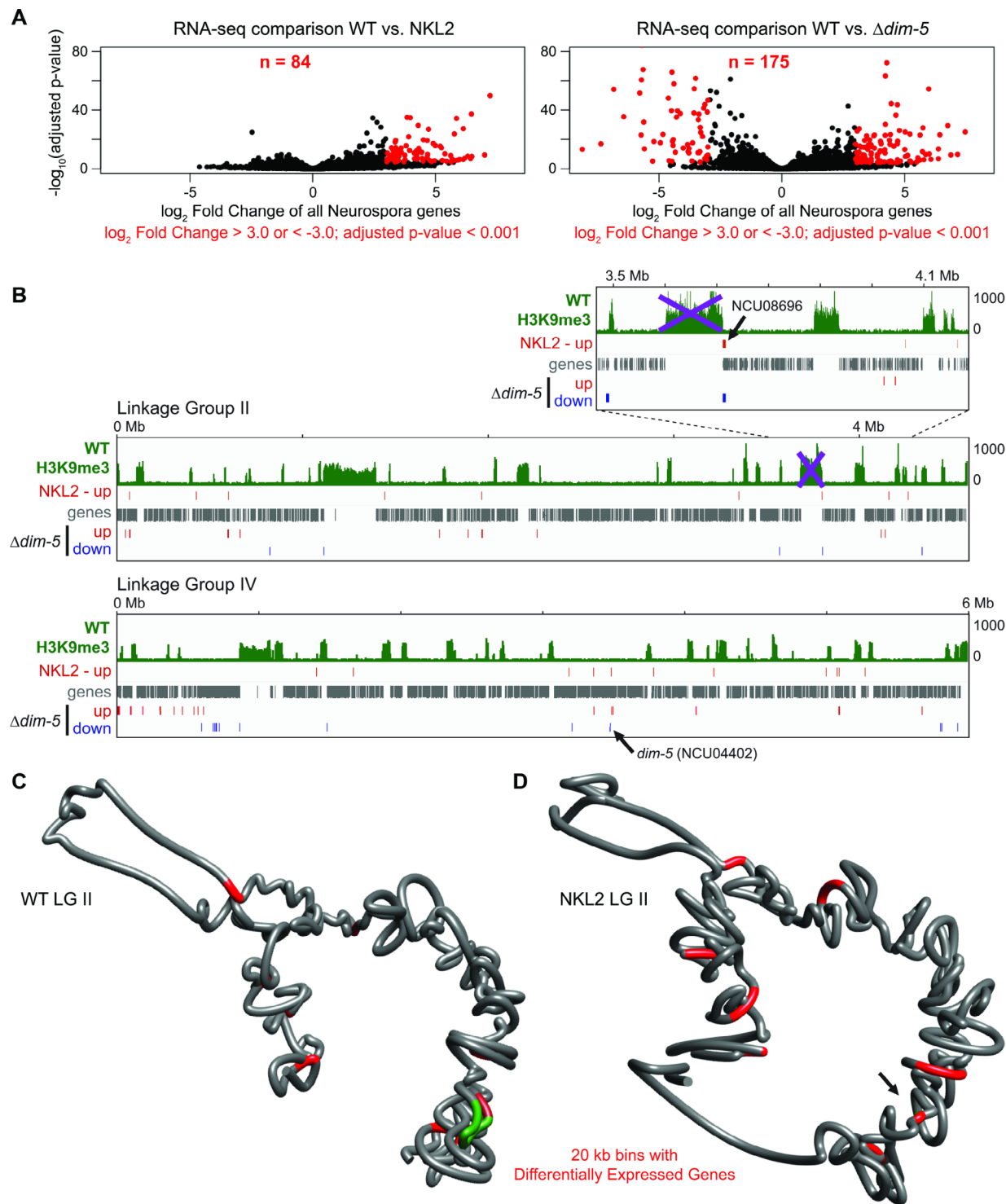


Fig. 6 The LGIIK9het25 region deletion causes increased gene expression genome wide. **(A)** Volcano plots showing the \log_2 fold change from WT expression levels of all Neurospora genes versus adjusted p-values from (left) the NKL2 Δ LGIIK9het25 or (right) the $\Delta dim-5$ strains. Red points are genes with significant expression changes (\log_2 fold changes > 3.0 or < -3.0 and adjusted p-values < 0.001). The number of differentially expressed genes (DEGs) is indicated at the top. **(B)** Images of IGV tracks showing WT H3K9me3 ChIP-seq (green), genes (gray), or the “up” ($\log_2 > 3.0$; red) or “down” ($\log_2 < -3.0$; blue) DEGs. The purple “X” symbols cover LGIIK9het25, which is deleted in the NKL2 strain, while the black arrows show the positions of genes NCU08696 or *dim-5* (NCU04402). **(C-D)** Images depicting the predicted 3D modeling of LG II from **(C)** WT or **(D)** NKL2 Δ LGIIK9het25 strains at 20 kb resolution. The green region highlights the LGIIK9het25 region in the WT structure, while 20 kb bins containing DEGs in the NKL2 strain, relative to a WT strain are colored red; the same bins are marked on both structures. The arrow in **D** shows the LGIIK9het25 deletion site

on each chromosome (Fig. 6B, S18), with many genes near H3K9me3-marked heterochromatic regions. To assess if linear chromosome distance between DEGs and heterochromatic regions affects gene expression, we measured the closest distance between each DEG transcription start site (TSS) and the nearest heterochromatic region border, plotting the distance in groups (from 1 to 1,000 bp; 1,001–10,000 bp; 10,001–100,000 bp; and 100,001–1 million [M] bp apart). Most DEGs ($n=51$) are 10,001–100,000 bp distant from the nearest H3K9me3-enriched border, with the second most DEGs ($n=23$) found up to 1 M bp distant (Figure S19), suggesting linear genomic distance has a minor regulatory role. The single gene within 1,000 bp of a heterochromatic region, NCU08696, is directly adjacent to LGIIK9het25 and is downregulated in the $\Delta dim-5$ strain but upregulated in Δ LGIIK9het25 (Fig. 6B, zoomed region), the latter possibly due to its proximity to the strong P_{trpC} promoter. While longer chromosomes would be expected to have more DEGs, the short ~ 4.3 Mb LG VII has more genes with changed expression ($n=24$ DEGs) than either the ~ 10 Mb LG I ($n=20$ DEGs) or the 6.0 Mb LG IV ($n=11$ DEGs) (Fig. 6B and S18, Supplementary File S2). We conclude that a single constitutive heterochromatic region impacts gene expression across the fungal genome.

To assess if altered 3D chromosome folding could explain the transcriptional changes in the Δ LGIIK9het25 strain, we colored bins harboring DEGs on NKL2 chromosome models. Qualitatively, the positions of the bins containing DEGs are modified on Δ LGIIK9het25 chromosome structures relative to the WT chromosomes

(Fig. 6C-D, S19, S20). Specifically, on LG II, the bins with DEGs appear more “enclosed” within the WT structure, while these same bins are repositioned to another “face” of the NKL2 LG II structure (Fig. 6C-D). Similar qualitative bin movements altering DEG positions are observed on other LGs (Figures S20-S21).

Finally, we examined the positions of Δ LGIIK9het25 DEGs relative to the 3D folding predicted for the entire WT and NKL2 genomes. Our 3D genome models maintain the biologically relevant [25, 37] single centromere cluster which is distinct from telomere bundles (Figure S22). The WT genome model forms an elongated structure with the LGIIK9het25 region close to the structure top (Fig. 7A), consistent with the “stretched” conformation of individual chromosomes (Fig. 5, 6C-D, S20-S21) and a previous report [68], despite different programs predicting each 3D structure. The NKL2 genome deleted of LGIIK9het25 is wider and less elongated (Fig. 7B), similar to the individual NKL2 chromosomes. Intriguingly, the 20 kb bins with Δ LGIIK9het25 DEGs are qualitatively oriented towards the WT genome periphery, while the same bins are more centrally localized in the NKL2 genome, consistent with a hypothesis where enhanced transcription machinery access increases gene expression (Fig. 7A-B). We conclude that the deletion of a single heterochromatic region alters the 3D genome conformation and disrupts normal genome function in the *Neurospora* nucleus.

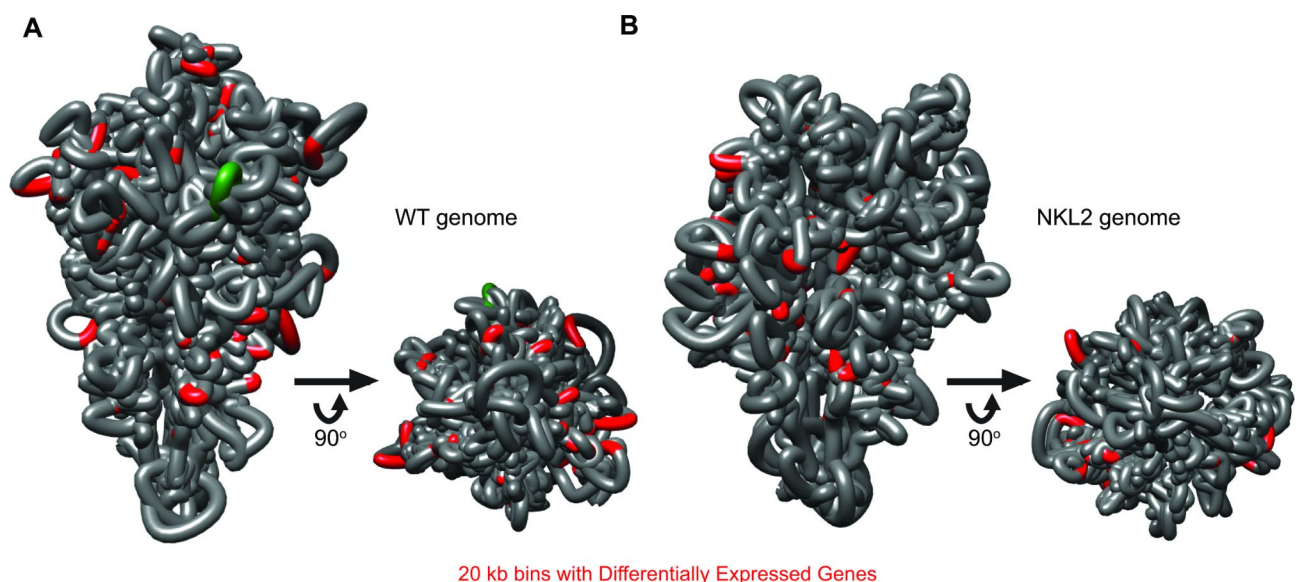


Fig. 7 The predicted 3D genome structure and DEG positions are altered upon LGIIK9het25 deletion. **(A-B)** Images depicting the predicted 3D genome structure of **(A)** WT or **(B)** NKL2 Δ LGIIK9het25 strains. The left image in each panel is the side view of the genome structure; the right image is where the genome structure is rotated up 90°, showing the centromere cluster. The green region highlights the LGIIK9het25 region in the WT structure, while the 20 kb bins containing DEGs in the NKL2 Δ LGIIK9het25 strain are colored red

Discussion

Here, we examined if facultative and constitutive heterochromatic regions organize the fungal genome by performing Hi-C on strains harboring silent region deletions. Our results suggest that gene-rich facultative heterochromatic loci are plastic in nature, as a facultative heterochromatin deletion simply fuses nearby H3K27me2/3-enriched regions within the linear chromosome, which minimally impacts facultative heterochromatin clusters. Specifically, the subtelomere bundling at the terminal ~150 kb of each LG is maintained in the Δ K27 strain. Subtelomere clustering may be compromised by larger deletions or deletions that target the terminal ~150 kb of chromosome ends. Consistent with these hypotheses, genome-wide loss of H3K27me2/3 in a *Neurospora* Δ set-7 (Δ kmt-6) strain can release subtelomere cluster(s) from the nuclear periphery [37], suggesting at least some subtelomeric H3K27me2/3 is needed for telomeres to associate with the nuclear membrane. It is possible that larger or more telomere-proximal deletions would disrupt subtelomere clustering, but further facultative heterochromatin deletions have not been attempted [34]. Still, it is likely that *Neurospora* tolerates alterations to gene-rich genomic loci, assuming no essential genes are deleted, given the absence of wide-ranging topological or physiological consequences. Since most genes enriched with H3K27me2/3 are novel genes with hypothetical functions [33], perhaps *Neurospora* tolerates subtelomeric structural variants if facultative heterochromatin is present. In contrast, some *Fusarium* species require H3K27me2/3 for normal growth [69], meaning structural variants in facultative heterochromatic regions may be lethal in other fungi.

We also assessed the role of a constitutive heterochromatic region for organizing the *Neurospora* genome. The most recent *Neurospora* reference genome (nc14) [24] has ~200 interspersed H3K9me3-enriched regions distributed over seven chromosomes, and apart from the centromeres and telomeres on each LG necessary for chromosome function, the remaining interspersed heterochromatic regions have been dismissed as “junk DNA”. However, when we delete the largest, non-centromeric heterochromatic region on LG II, genome organization and function are impacted without a severe phenotypic effect. Specifically, the heterochromatic regions still present in NKL2 uniquely cluster when LGIIK9het25 is deleted, as we observe gains in intra- and inter-chromosomal heterochromatin contacts, including between interspersed heterochromatic regions and centromeres. Any altered inter-heterochromatic region bundling may reflect valid genome organization changes in NKL2 nuclei, as hypothetically, the LGIIK9het25 deletion would cause the remaining interspersed heterochromatic regions to form novel and variable inter-heterochromatin

contacts in each nucleus. These organizational changes may then be amplified by the Hi-C protocol, resulting in the increased contact probability variation we observe. Therefore, a limitation of this study is that we cannot differentiate between these two sources of variability. Still, since genome organization can vary between individual cells across a population [70], it is likely that LGIIK9het25 removal causes contact probability matrix variation from altered heterochromatin bundling. Future controlled fungal Hi-C experiments coupled with computational modeling are warranted to assess the day-to-day Hi-C experiment variability to shed light on valid genome organization changes in WT and Δ LGIIK9het25 strains. Nevertheless, LGIIK9het25 appears to primarily have a structural role in anchoring silent regions on *Neurospora* chromosomes, while other heterochromatic regions may impact genome function to a greater extent. Additional H3K9me3-enriched region deletions, or progressive truncations of LGIIK9het25, could have elucidated other effects on heterochromatin bundling or fungal genome function. Further, it is possible that additional WT or NKL2 genome organization or function effects could have been discovered with different growth conditions, such as alternative carbon or nitrogen sources, osmolarities, or temperatures, in a manner synonymous to the jet-like chromatin structures across secondary metabolite clusters observed when *Fusarium graminearum* is cultured in excess nitrogen [71].

Our Δ LGIIK9het25 data favor a model where the *Neurospora* heterochromatin bundle is dynamic, but we cannot exclude the possibility that proteins binding to specific DNA motifs in AT-rich DNA promote heterochromatin aggregation. We suggest that any dynamic heterochromatin clustering could be mediated by Liquid Liquid Phase Separation or a chromatin binding protein, such as Heterochromatin Protein-1 (HP1) [72–74]. Since HP1 loss does not radically disrupt the *Neurospora* heterochromatin bundle [25], multiple factors, acting redundantly, could drive fungal heterochromatin aggregation. Consistent with this hypothesis, HP1-independent pericentromere clusters are observed in *Drosophila* [75]. It is currently unknown how eukaryotic constitutive heterochromatic regions bundle, although histone post-translational modifications and/or DNA methylation contribute to fungal genome organization. Specifically in *Neurospora*, subtelomeric H3K27me2/3 loss causes genome disorder and reduced telomere tethering, while deletion of the HCHC histone deacetylase complex causes constitutive heterochromatin hyperacetylation to increase inter-heterochromatic region contacts; heterochromatin hyperacetylation coupled with 5^mC loss reduces heterochromatin compartmentalization [37, 47]. Future experiments should elucidate other chromatin-specific mechanisms for organizing eukaryotic genomes.

The LGIIK9het25 deletion also changes local chromatin structure and 3D genome folding. In a manner synonymous to the $\Delta K27$ strain, the LGIIK9het25 deletion fuses flanking chromatin segments, as shown by contact gains between neighboring euchromatin bins. However, this deletion of LGIIK9het25 alters the predicted TADs, and therefore the regional chromatin looping, across the fused chromatin in two TAD prediction programs. Since interspersed heterochromatic regions in filamentous fungi anchor the bases of TAD-like structures [9, 24–26, 36], in a mechanism tantamount to CTCF forming metazoan loops [10], removing a heterochromatic region could allow interactions between distant euchromatic regions. However, the extensive inter-TAD interactions in fungi [24–26] complicate TAD prediction, and non-uniform TAD-like structures in a single *Neurospora* nucleus could minimize the functional consequences of altered chromatin loops. While we used TAD prediction parameters to keep heterochromatic region TADs in domains of H3K9me3 to accurately report biologically relevant TADs, one limitation of our study is that euchromatic TAD/loop prediction is particularly challenging in *Neurospora*. In fact, variable intra- and inter-heterochromatin bundling across chromosomes could cause variability in euchromatin loops in nuclei populations, similar to the variable TAD boundaries reported in different human cell types [76]. Still, our study has functional implications for higher eukaryotic systems. While fungi and metazoans employ some unique chromatin folding mechanisms, the deletion of a metazoan constitutive heterochromatic region could also disrupt TADs to promote new contacts across the normally isolated TAD-internal chromatin, in a manner synonymous to our results in fungi. Thus, loss of a H3K9me3-enriched region from a metazoan genome could alter TAD compartmentalization or misregulate gene expression if several smaller TADs are merged into a larger TAD. Unfortunately, the consequences to metazoan genome function would be more dire, given how TAD boundary dysfunction compromises proper gene expression [6–8]. In fact, our chromosome and genome structure predictions suggest local looping changes could manifest into a unique folding pattern for the entire genome. Here, the Δ LGIIK9het25 deletion caused each chromosome, and the genome, to qualitatively form conformations distinct from the WT genome. While these models are merely predictions and should be interpreted lightly, it is impactful that the repositioning of a single locus has the potential to alter the 3D structure of a whole genome. Hypothetically, despite the species-specific differences in TADs or loops, syntetic changes of linear chromosomal DNA could disorganize a species' genome, causing functional changes.

Our results also suggest a single constitutive heterochromatic region impacts the transcription of distant

genes in the WT *Neurospora* genome. The gene expression changes we observe in the LGIIK9het25 deletion differ from those in a $\Delta dim-5$ strain if all H3K9me3 is removed, the latter strain causing numerous genes to become strongly up- or down-regulated [37], suggesting LGIIK9het25 has a minor but real impact on genome function. Overall, this single constitutive heterochromatic region may subtly repress *Neurospora* gene expression. Control of gene expression by H3K9me3-enriched regions in *Neurospora* was hypothesized from observations of strong contacts between genes and constitutive heterochromatic regions in high-resolution Hi-C datasets [24]. However, it is difficult to imagine that a single LGIIK9het25 region deletion directly causes gene expression changes genome wide. More likely, the Δ LGIIK9het25 allele alters the positioning of the heterochromatin bundle – and the nearby euchromatin – at the nuclear periphery, which repositions some gene promoters for increased transcription machinery accessibility. This hypothesis is supported by modeling the gene expression changes on the Δ LGIIK9het25 chromosomes and across the genome and reasonably explains gene activation in the NKL2 strain. Of course, altered promoters can also drive gene expression changes, as observed by the strong P_{trpC} promoter in the NKL2 deletion strain increasing the transcription of gene NCU08696 immediately adjacent to LGIIK9het25, although the possibility exists that these changes are a consequence of the loss of AT-rich DNA. In contrast, NCU08696, and other genes near constitutive heterochromatic regions, are down-regulated in the $\Delta dim-5$ strain lacking H3K9me3, suggesting that some H3K9me3-enriched regions directly control transcription. Similarly, the proper expression of the *Neurospora met-8* gene requires the immediately adjacent interspersed constitutive heterochromatic region [77]. Together, our results show gene regulation across the fungal genome – even genes on different chromosomes – may depend on a single constitutive heterochromatic region. In metazoans, H3K9me3 enrichment at a gene promoter can repress expression, as the control of mouse embryonic stem cell identity requires the co-deposition of H3K9me3 and H3K36me3 for transcriptional repression [78]. Thus, in addition to the canonical repression of transposable elements and repetitive sequences in eukaryotic genomes [79–82], H3K9me3 can directly regulate transcription. We propose that heterochromatin-mediated gene regulation also occurs through 3D organization, where genes interact with H3K9me3-enriched regions. In this model, genes would associate with constitutive heterochromatic regions at the more repressive periphery for reducing transcription; should these genes be reoriented to the active nuclear center, transcription would increase. It is feasible that constitutive heterochromatic regions could indirectly

regulate more “evolutionarily new” or fungal specific genes, in a similar manner as facultative heterochromatin in *Neurospora* [33], and examining all genes regulated by constitutive heterochromatin in RNA-seq datasets from multiple region deletion strains could assess the evolutionary age of genes controlled by H3K9me3-marked regions. Currently, it is unknown how constitutive heterochromatic regions may regulate gene expression, but an attractive model includes HP1 binding to small amounts of H3K9me3 deposited at gene promoters to allow aggregation with the constitutive heterochromatin bundle; the amount of H3K9me3 needed to implement this regulation is unknown, but could be minor or occur only in a sub-population of nuclei, given the near background levels of H3K9me3 across *Neurospora* genic regions in ChIP-seq of mycelial populations. Still, fungi may be more apt to employ this hypothetical mechanism to regulate transcription, as opposed to metazoans, given the more-promiscuous contacts across fungal TAD-like structures and the extensive inter-chromosomal contacts in the Rabl chromosome conformation in fungi [9, 24–26, 36]. Recently, the histone methyltransferase SETDB1, which catalyzes H3K9me3 in metazoans, was shown to maintain gene expression and drive chromatin compartmentalization [83]. Thus, constitutive heterochromatic regions have additional, underappreciated roles in both genome organization and function across diverse species.

Conclusions

Our work here has directly assessed how one large H3K9me3-marked silent genomic region impacts fungal genome organization and function. Here, the deletion of a 110.6 kb H3K9me3-enriched region alters the hierarchical 3D genome organization in *Neurospora crassa*, with chromatin fibers, TAD-like structures, individual chromosomes, and the fungal genome all having altered conformations. The H3K9me3 deposition on neighboring gene poor regions still occurs despite this 110.6 kb constitutive heterochromatic region deletion, yet this deletion increases gene expression genome wide, which 3D genome modeling suggests is due to upregulated genes being mispositioned into the transcriptionally active nucleus center. Since the *Neurospora* genome contains 200+ other H3K9me3-regions, it is likely that each silent region similarly contributes to genome function. Since many eukaryotic genomes have H3K9me3-enriched constitutive heterochromatic regions, including many metazoans, the aggregation of constitutive heterochromatin may be a conserved mechanism for organizing eukaryotic genomes and that individual H3K9me3-enriched regions may regulate eukaryotic transcription. Further research in multiple species should help elucidate novel functional roles for this pervasive yet evolutionarily conserved “junk DNA” retained in eukaryotic genomes.

Supplementary Information

The online version contains supplementary material available at <https://doi.org/10.1186/s12864-024-11110-7>.

- Supplementary Material 1
- Supplementary Material 2
- Supplementary Material 3
- Supplementary Material 4
- Supplementary Material 5

Acknowledgements

The authors thank Sara Rodriguez, Yulia Shtanko, and Ashley Scadden for Hi-C library generation help; Sara Hanson (Colorado College) for TapeStation use and RNA-seq protocol advice; the University of Oregon GC3F for Illumina library sequencing service, and Klocko lab members and UCCS Department of Chemistry & Biochemistry colleagues for helpful comments and discussions.

Author contributions

A.T.R. and A.D.K. designed research; A.T.R., A.P., J.V., C.G.C., O.O. and A.D.K. performed research; A.T.R., A.P., J.V., C.G.C., O.O. and A.D.K. analyzed data; and A.T.R., A.P., J.V., C.G.C., O.O. and A.D.K. wrote the paper.

Funding

Funding was provided by a UCCS Undergraduate Research Academy award to A.T.R., National Science Foundation (NSF) CRII Award (Grant No. 2153205) awarded to O.O., a National Institutes of Health (NIH) Maximizing Investigators Research Award grant (1R35GM150402-01) to O.O., start-up funds from the UCCS College of Letters, Arts, and Sciences to A.D.K., and a NIH Academic Research Enhancement Award grant (1R15GM140396-01) to A.D.K.

Data availability

All genomic datasets are deposited in the NCBI GEO under the SuperSeries accession number GSE269235. Individual datasets have the subseries numbers GSE269228 (ChIP-seq), GSE269229 (Hi-C), and GSE269230 (polyA mRNA-seq). All *Neurospora* strains are available upon request.

Declarations

Ethics approval and consent to participate

Not applicable.

Consent for publication

Not applicable.

Competing interests

The authors declare no competing interests.

Received: 13 June 2024 / Accepted: 2 December 2024

Published online: 20 December 2024

References

- Cremer T, Cremer C. Chromosome territories, nuclear architecture and gene regulation in mammalian cells. *Nat Rev Genet*. 2001;2:292–301.
- Misteli T. Beyond the sequence: Cellular Organization of genome function. *Cell*. 2007;128:787–800.
- Dekker J. Gene Regulation in the third dimension. *Science*. 2008;319:1793–4.
- Sexton T, Cavalli G. The role of chromosome domains in shaping the functional genome. *Cell*. 2015;160:1049–59.
- Bonev B, Cavalli G. Organization and function of the 3D genome. *Nat Rev Genet*. 2016;17:661–78.
- Flavahan WA, Drier Y, Liao BB, Gillespie SM, Venteicher AS, Stemmer-Rachamim AO, et al. Insulator dysfunction and oncogene activation in IDH mutant gliomas. *Nature*. 2016;529:110–4.

7. Dixon JR, Xu J, Dileep V, Zhan Y, Song F, Le VT, et al. Integrative detection and analysis of structural variation in cancer genomes. *Nat Genet*. 2018;50:1388–98.
8. Northcott PA, Lee C, Zichner T, Stütz AM, Erkek S, Kawauchi D, et al. Enhancer hijacking activates GF1 family oncogenes in medulloblastoma. *Nature*. 2014;511:428–34.
9. Torres DE, Reckard AT, Klocko AD, Seidl MF. Nuclear genome organization in fungi: from gene folding to Rabl chromosomes. *FEMS Microbiol Rev*. 2023;47(3):fua021.
10. Rao SSP, Huntley MH, Durand NC, Stamenova EK, Bochkov ID, Robinson JT, et al. A 3D map of the Human Genome at Kilobase Resolution reveals principles of chromatin looping. *Cell*. 2014;159:1665–80.
11. Lieberman-Aiden E, van Berkum NL, Williams L, Imakaev M, Ragoczy T, Telling A, et al. Comprehensive mapping of long-range interactions reveals folding principles of the Human Genome. *Science*. 2009;326:289–93.
12. Luger K, Mäder AW, Richmond RK, Sargent DF, Richmond TJ. Crystal structure of the nucleosome core particle at 2.8 Å resolution. *Nature*. 1997;389:251–60.
13. Luger K, Richmond TJ. DNA binding within the nucleosome core. *Curr Opin Struct Biol*. 1998;8:33–40.
14. Rao SSP, Huang S-C, Hilaire BGS, Engreitz JM, Perez EM, Kieffer-Kwon K-R, et al. Cohesin Loss Eliminates all Loop Domains Cell. 2017;171:305–e3204.
15. Mizuguchi T, Fudenberg G, Mehta S, Belton J-M, Taneja N, Folco HD, et al. Cohesin-dependent globules and heterochromatin shape 3D genome architecture in *S. pombe*. *Nature*. 2014;516:432–5.
16. Campos EI, Reinberg D. Histones: Annotating chromatin. *Annu Rev Genet*. 2009;43:559–99.
17. Dixon JR, Selvaraj S, Yue F, Kim A, Li Y, Shen Y, et al. Topological domains in mammalian genomes identified by analysis of chromatin interactions. *Nature*. 2012;485:376–80.
18. Kind J, Pagie L, de Vries SS, Nahidazar L, Dey SS, Bienko M, et al. Genome-wide maps of nuclear Lamina interactions in single human cells. *Cell*. 2015;163:134–47.
19. Falk M, Feodorova Y, Naumova N, Imakaev M, Lajoie BR, Leonhardt H, et al. Heterochromatin drives compartmentalization of inverted and conventional nuclei. *Nature*. 2019;570:395–9.
20. Schoenfelder S, Sexton T, Chakalova L, Cope NF, Horton A, Andrews S, et al. Preferential associations between co-regulated genes reveal a transcriptional interactome in erythroid cells. *Nat Genet*. 2010;42:53–61.
21. Mahajan A, Yan W, Zidovska A, Saintillan D, Shelley MJ. Euchromatin activity enhances segregation and compaction of heterochromatin in the cell nucleus. *Phys Rev X*. 2022;12:041033.
22. Hoencamp C, Dudchenko O, Elbatsh AMO, Brahmachari S, Raaijmakers JA, van Schaik T, et al. 3D genomics across the tree of life reveals condensin II as a determinant of architecture type. *Science*. 2021;372:984–9.
23. Imakaev M, Fudenberg G, McCord RP, Naumova N, Goloborodko A, Lajoie BR, et al. Iterative correction of Hi-C data reveals hallmarks of chromosome organization. *Nat Methods*. 2012;9:999–1003.
24. Rodriguez S, Ward A, Reckard AT, Shtanko Y, Hull-Crew C, Klocko AD. The genome organization of *Neurospora crassa* at high resolution uncovers principles of fungal chromosome topology. *G3: Genes Genomes Genetics*. 2022;12(5):jkac053.
25. Galazka JM, Klocko AD, Uesaka M, Honda S, Selker EU, Freitag M. Neurospora chromosomes are organized by blocks of importin alpha-dependent heterochromatin that are largely independent of H3K9me3. *Genome Res*. 2016;26:1069–80.
26. Torres DE, Kramer HM, Tracanna V, Fiorin GL, Cook DE, Seidl MF, et al. Implications of the three-dimensional chromatin organization for genome evolution in a fungal plant pathogen. *Nat Commun*. 2023;15:1701.
27. Galagan JE, Calvo SE, Borkovich KA, Selker EU, Read ND, Jaffe D, et al. The genome sequence of the filamentous fungus *Neurospora crassa*. *Nature*. 2003;422:859–68.
28. Lewis ZA, Honda S, Khalfallah TK, Jeffress JK, Freitag M, Mohn F, et al. Relics of repeat-induced point mutation direct heterochromatin formation in *Neurospora crassa*. *Genome Res*. 2009;19:427–37.
29. Nurk S, Koren S, Rhee A, Rautiainen M, Bzikadze AV, Mikheenko A, et al. The complete sequence of a human genome. *Science*. 2022;376:44–53.
30. Tamari H, Zhang X, McMillen D, Singh PB, Nakayama J, Grewal SI, et al. Trimethylated lysine 9 of histone H3 is a mark for DNA methylation in *Neurospora crassa*. *Nat Genet*. 2003;34:75–9.
31. Lewis ZA, Adhvaryu KK, Honda S, Shiver AL, Knip M, Sack R, et al. DNA methylation and normal chromosome behavior in *Neurospora* Depend on five components of a Histone Methyltransferase Complex, DCDC. *PLoS Genet*. 2010;6:e1001196.
32. Klocko AD, Uesaka M, Ormsby T, Rountree MR, Wiles ET, Adhvaryu KK, et al. Nucleosome positioning by an evolutionarily conserved chromatin remodeler prevents aberrant DNA methylation in *Neurospora*. *Genetics*. 2019;211:563–78.
33. Jamieson K, Rountree MR, Lewis ZA, Stajich JE, Selker EU. Regional control of histone H3 lysine 27 methylation in *Neurospora*. *Proc Natl Acad Sci*. 2013;110:6027–32.
34. Jamieson K, McNaught KJ, Ormsby T, Leggett NA, Honda S, Selker EU. Telomere repeats induce domains of H3K27 methylation in *Neurospora*. *Elife*. 2018;7:e31216.
35. Wiles ET, Selker EU. H3K27 methylation: a promiscuous repressive chromatin mark. *Curr Opin Genet Dev*. 2017;43:31–7.
36. Winter DJ, Ganley ARD, Young CA, Liachko I, Schardl CL, Dupont P-Y, et al. Repeat elements organise 3D genome structure and mediate transcription in the filamentous fungus *Epichloë festucae*. *PLoS Genet*. 2018;14:e1007467.
37. Klocko AD, Ormsby T, Galazka JM, Leggett NA, Uesaka M, Honda S, et al. Normal chromosome conformation depends on subtelomeric facultative heterochromatin in *Neurospora crassa*. *Proc Natl Acad Sci*. 2016;113:15048–53.
38. Davis RH. *Neurospora*: contributions of a model organism. Oxford University Press; 2000.
39. Honda S, Selker EU. Tools for fungal proteomics: multifunctional neurospora vectors for gene replacement, protein expression and protein purification. *Genetics*. 2009;182:11–23.
40. Miao VPW, Freitag M, Selker EU. Short TpA-rich segments of the ζ - η region induce DNA methylation in *Neurospora crassa*. *J Mol Biol*. 2000;300:249–73.
41. Langmead B, Salzberg SL. Fast gapped-read alignment with Bowtie 2. *Nat Methods*. 2012;9:357–9.
42. Ramirez F, Bhardwaj V, Arrigoni L, Lam KC, Grüning BA, Villaveces J, et al. High-resolution TADs reveal DNA sequences underlying genome organization in flies. *Nat Commun*. 2018;9:189.
43. Shin H, Shi Y, Dai C, Tjong H, Gong K, Alber F, et al. TopDom: an efficient and deterministic method for identifying topological domains in genomes. *Nucleic Acids Res*. 2016;44:e70–70.
44. Oluwadare O, Zhang Y, Cheng J. A maximum likelihood algorithm for reconstructing 3D structures of human chromosomes from chromosomal contact data. *BMC Genom*. 2018;19:161.
45. Trieu T, Cheng J. 3D genome structure modeling by lorentzian objective function. *Nucleic Acids Res*. 2017;45:1049–58.
46. Pettersen EF, Goddard TD, Huang CC, Meng EC, Couch GS, Croll TI, et al. UCSF ChimeraX: structure visualization for researchers, educators, and developers. *Protein Sci*. 2021;30:70–82.
47. Scadden AW, Graybill AS, Hull-Crew C, Lundberg TJ, Lande NM, Klocko AD. Histone deacetylation and cytosine methylation compartmentalize heterochromatic regions in the genome organization of *Neurospora crassa*. *Proc Natl Acad Sci*. 2023;120:e2311249120.
48. Li H, Handsaker B, Wysoker A, Fennell T, Ruan J, Homer N, et al. The sequence Alignment/Map format and SAMtools. *Bioinformatics*. 2009;25:2078–9.
49. Ramirez F, Ryan DP, Grüning B, Bhardwaj V, Kilpert F, Richter AS, et al. deepTools2: a next generation web server for deep-sequencing data analysis. *Nucleic Acids Res*. 2016;44:W160–5.
50. Robinson JT, Thorvaldsdóttir H, Winckler W, Guttman M, Lander ES, Getz G, et al. Integrative genomics viewer. *Nat Biotechnol*. 2011;29:24–6.
51. Jamieson K, Wiles ET, McNaught KJ, Sidoli S, Leggett N, Shao Y, et al. Loss of HP1 causes depletion of H3K27me3 from facultative heterochromatin and gain of H3K27me2 at constitutive heterochromatin. *Genome Res*. 2016;26:97–107.
52. Basenko EY, Sasaki T, Ji L, Prybol CJ, Burckhardt RM, Schmitz RJ, et al. Genome-wide redistribution of H3K27me3 is linked to genotoxic stress and defective growth. *Proc Natl Acad Sci*. 2015;112:E6339–48.
53. Klocko AD, Summers CA, Glover ML, Parrish R, Storch WK, McNaught KJ, et al. Selection and characterization of mutants defective in DNA methylation in *Neurospora crassa*. *Genetics*. 2020;216:genetics.303471.2020.
54. Kamei M, Ameri AJ, Ferraro AR, Bar-Peled Y, Zhao F, Ethridge CL, et al. IMITATION SWITCH is required for normal chromatin structure and gene repression in PRC2 target domains. *Proc Natl Acad Sci*. 2021;118:e2010003118.
55. Zhang Y, Park C, Bennett C, Thornton M, Kim D. Rapid and accurate alignment of nucleotide conversion sequencing reads with HISAT-3 N. *Genome Res*. 2020;31:1290–5.
56. Anders S, Pyl PT, Huber W. HTSeq—a Python framework to work with high-throughput sequencing data. *Bioinform Oxf Engl*. 2015;31:166–9.

57. Love MI, Huber W, Anders S. Moderated estimation of Fold change and dispersion for RNA-seq data with DESeq2. *Genome Biol.* 2014;15:550.

58. Team Rs. RStudio: Integrated Development for R. Boston, MA: RStudio, PBC; 2020.

59. Team RC. R: a language and environment for statistical computing. Vienna, Austria: R Foundation for Statistical Computing; 2021.

60. Knight PA, Ruiz D. A fast algorithm for matrix balancing. *IMA J Numer Anal.* 2013;33:1029–47.

61. Ninomiya Y, Suzuki K, Ishii C, Inoue H. Highly efficient gene replacements in *Neurospora* strains deficient for nonhomologous end-joining. *Proc Natl Acad Sci.* 2004;101:12248–53.

62. Selker E. Premeiotic instability of repeated sequences in *Neurospora crassa*. *Annu Rev Genet.* 1990;24:579–613.

63. Gladyshev E, Kleckner N. Direct recognition of homology between double helices of DNA in *Neurospora crassa*. *Nat Commun.* 2014;5:3509–3509.

64. Kück U, Hoff B. Application of the nourseothricin acetyltransferase gene (nat1) as dominant marker for the transformation of filamentous fungi. *Fungal Genet Rep.* 2006;53:9–11.

65. Bonhoure N, Bounova G, Bernasconi D, Praz V, Lammers F, Canella D, et al. Quantifying ChIP-seq data: a spiking method providing an internal reference for sample-to-sample normalization. *Genome Res.* 2014;24:1157–68.

66. Orlando DA, Chen MW, Brown VE, Solanki S, Choi YJ, Olson ER, et al. Quantitative ChIP-Seq normalization reveals global modulation of the Epigenome. *Cell Rep.* 2014;9:1163–70.

67. Zufferey M, Tavernari D, Oricchio E, Ciriello G. Comparison of computational methods for the identification of topologically associating domains. *Genome Biol.* 2018;19:217.

68. Poinsignon T, Gallopin M, Grognat P, Malagnac F, Lelandais G, Poulain P. 3D models of fungal chromosomes to enhance visual integration of omics data. *NAR Genom Bioinform.* 2023;5:lgad104.

69. Connolly LR, Smith KM, Freitag M. The *Fusarium graminearum* histone H3 K27 methyltransferase KMT6 regulates Development and expression of secondary metabolite gene clusters. *PLoS Genet.* 2013;9:e1003916.

70. Nagano T, Lubling Y, Stevens TJ, Schoenfelder S, Yaffe E, Dean W, et al. Single-cell Hi-C reveals cell-to-cell variability in chromosome structure. *Nature.* 2013;502:59–64.

71. Shao W, Wang J, Zhang Y, Zhang C, Chen J, Chen Y, et al. The jet-like chromatin structure defines active secondary metabolism in fungi. *Nucleic Acids Res.* 2024;52:4906–21.

72. Larson AG, Elnatan D, Keenen MM, Trnka MJ, Johnston JB, Burlingame AL, et al. Liquid droplet formation by HP1a suggests a role for phase separation in heterochromatin. *Nature.* 2017;547:236–40.

73. Freitag M, Hickey PC, Khalfallah TK, Read ND, Selker EU. HP1 is essential for DNA methylation in *Neurospora*. *Mol Cell.* 2004;13:427–34.

74. Zenk F, Zhan Y, Kos P, Löser E, Atinbayeva N, Schächtle M, et al. HP1 drives *de novo* 3D genome reorganization in early *Drosophila* embryos. *Nature.* 2021;593:289–93.

75. Stutzman AV, Hill CA, Armstrong RL, Gohil R, Duronio RJ, Dowen JM, et al. Heterochromatic 3D genome organization is directed by HP1a- and H3K9-dependent and independent mechanisms. *Mol Cell.* 2024;84(11):2017–e356.

76. Sauerwald N, Singhal A, Kingsford C. Analysis of the structural variability of topologically associated domains as revealed by Hi-C. *NAR Genom Bioinform.* 2019;2:lgz008.

77. Yang S, Li W, Qi S, Gai K, Chen Y, Suo J, et al. The highly expressed methionine synthase gene of *Neurospora crassa* is positively regulated by its proximal heterochromatic region. *Nucleic Acids Res.* 2014;42:6183–95.

78. Barral A, Pozo G, Ducrot L, Papadopoulos GL, Sauzet S, Oldfield AJ, et al. SETDB1/NSD-dependent H3K9me3/H3K36me3 dual heterochromatin maintains gene expression profiles by bookmarking poised enhancers. *Mol Cell.* 2022;82:816–e83212.

79. Padeken J, Zeller P, Towbin B, Katic I, Kalck V, Methot SP, et al. Synergistic lethality between BRCA1 and H3K9me2 loss reflects satellite derepression. *Genes Dev.* 2019;33:436–51.

80. Padeken J, Methot SP, Gasser SM. Establishment of H3K9-methylated heterochromatin and its functions in tissue differentiation and maintenance. *Nat Rev Mol Cell Biol.* 2022;23:623–40.

81. Herberg S, Simeone A, Oikawa M, Jullien J, Bradshaw CR, Teperek M, et al. Histone H3 lysine 9 trimethylation is required for suppressing the expression of an embryonically activated retrotransposon in *Xenopus laevis*. *Sci Rep.* 2015;5:14236.

82. Zhao S, Lu J, Pan B, Fan H, Byrum SD, Xu C, et al. TNRC18 engages H3K9me3 to mediate silencing of endogenous retrotransposons. *Nature.* 2023;623:633–42.

83. Keenan CR, Coughlan HD, Iannarella N, del Fierro AT, Keniry A, Johanson TM, et al. Suv39h-catalyzed H3K9me3 is critical for euchromatic genome organization and the maintenance of gene transcription. *Genome Res.* 2024;34:556–71.

Publisher's note

Springer Nature remains neutral with regard to jurisdictional claims in published maps and institutional affiliations.